

A top-down approach to mechanistic biological
modeling: application to single-chain antibody
folding

Scott Hildebrandt

Department of Chemical Engineering,
University of California, Santa Barbara, CA

David Raden

Department of Chemical Engineering,
University of Delaware, Newark, DE

Linda Petzold

Department of Computer Science,
University of California, Santa Barbara, CA

Anne Skaja Robinson

Department of Chemical Engineering,
University of Delaware, Newark, DE

Francis J. Doyle, III¹

Department of Chemical Engineering,
University of California, Santa Barbara, CA

¹Corresponding author. Address: Department of Chemical Engineering, Uni-

Abstract

A top-down approach to mechanistic modeling of biological systems is presented and exemplified with the development of a mathematical model for single-chain antibody fragment (scFv) folding in *Saccharomyces cerevisiae* by mediators BiP and PDI. In this approach, model development starts with construction of the most basic mathematical model—typically consisting of predetermined or newly-elucidated biological behavior motifs—capable of reproducing desired biological behaviors. From this point, mechanistic detail is added incrementally and systematically, and the effects of these additions are evaluated with each increment. Use of this approach provides the modeler with an unprecedented intimacy with the structural requirements and performance capabilities of the resulting detailed mechanistic model, which complements and facilitates further analysis. The top-down approach to mechanistic modeling identified three such requirements and a branched dependency-degradation competition motif critical for the scFv folding model to reproduce experimentally-observed scFv folding dependencies on and synergy between BiP and PDI and promoted straightforward prediction and evaluation of parameter dependencies.

Key words: systems biology; mathematical modeling; top-down approach; protein folding; single-chain antibody; *Saccharomyces cerevisiae*

Introduction

In systems biology, mathematical models are used to describe biological systems in order to obtain understanding of system behavior and predict system responses (1). The type of model used and its scale and scope vary with the desired behaviors and responses it is intended to capture and predict, the desired level of detail, and the size of the biological system of interest. Model types range from the highest-level regulatory graphs, which show how species interact, to Bayesian networks, which represent conditional interactions and dependencies, to Boolean models, which describe switching behavior, to nonlinear ODE models, which describe dynamic behavior, to the most highly detailed stochastic models, which capture random behavior caused by low molecule counts (2–4). Model scale may range from molecular to organismal, and from low-level mechanistic detail to higher-level lumped behavioral units. Model building on the mechanistic scale has been referred to as “bottom-up,” as the model includes previously-known interactions and regulatory feedbacks, which are pared down as analysis identifies the critical, behavior-defining ones. Building on the more abstract, lumped behavioral scale has been referred to as “top-down,” where input-output relations are used to identify and gradually fill in previously unknown interactions (5). This work combines these two approaches by applying the top-down methodology to biological model building on the mechanistic scale.

By and large, mechanistic modeling approaches have not been formalized and are as varied as the models and biological systems under study themselves. Additionally, no formal evaluation of the approaches’ applicability

to or advantages in modeling a particular biological system has been performed. The body of circadian rhythm mathematical models demonstrates the variety of approaches that have been employed to describe a system largely conserved across mammals and fruit flies. In developing their mathematical model for the mammalian circadian rhythm, Forger and Peskin (6) performed an exhaustive literature search to include many of the known molecular interactions and mechanisms involved in the circadian clock, when a basic negative feedback loop was all that was necessary to reproduce experimentally-observed oscillations. This approach is clearly in the vein of bottom-up model building, and it produced a mathematical model containing 73 states and 74 parameters. In stark contrast, Tyson et al. (7) sought to capture and analyze circadian behavior in *Drosophila melanogaster* with a higher-level model by reducing a three-state model consisting of mRNA and two forms (monomer and dimer) of protein to two: mRNA and total protein. Meantime, Leloup and Goldbeter developed 10-state *Drosophila* (8) and 19-state mammalian (9) models of intermediate complexity to fulfill their analytical purposes.

Still, one generalized approach to mechanistic modeling of biological systems has been proposed (10): start by identifying all of the reactions within the scope of the biological system and perform mass balances around the participating species. Then, simplify the resulting mathematical model consisting of a set of nonlinear ODEs with further assumptions and approximations, which often leads to algebraic expressions, Michaelis-Menton kinetics, and transfer functions such as the Hill function. Finally, employ analytical tools such as sensitivity analysis to identify components responsible for

producing certain behaviors and stability and bifurcation analysis to assess what behaviors the system is capable of producing. This process description formalizes the bottom-up approach mechanistic model building.

This work describes a contrasting approach similar to that outlined by Ideker and Lauffenburger (11), but on the scale of mechanistic modeling: with the full desired mechanistic scope of the model defined, develop the simplest imaginable representation of the biological system in an attempt to isolate the “backbone” structure and identify motifs responsible for the underlying behavior. Once this basic model has been established, *gradually* expand it to include the desired mechanistic details, so the contributions—or lack thereof—of these modifications to system behavior may be incrementally evaluated using systems biology analytical tools. (In the cited work by Ideker and Lauffenburger (11), a top-down approach to biological modeling across many levels of complexity, starting from high-level regulatory graphs and gradually appending them with more data to transition to lower-level model types like ODE models, is described.) This approach may then be referred to as a top-down approach to mechanistic modeling, and its methodology is outlined in Figure 1. **This approach’s strength lies in the fact that it provides the modeler with an unprecedented intimacy with the behavioral contributions of each mechanistic component of the model.**

The top-down mechanistic modeling approach also benefits from the growing catalog of known biological motifs and modules responsible for producing certain biological behaviors. The *Escherichia coli* toggle switch (12) and repressilator (13) are two well-known examples from synthetic biology. Other examples include positive feedback loops that can store information

from transient signals, inhibitory feedback loops that guard against noise, and feed-forward loops that accelerate responses (14). Familiarity with these motifs and modules can aid in construction of the basic backbone structure by allowing one to identify more readily the components and interactions that will be necessary to reproduce experimentally-observed behaviors.

To demonstrate the top-down approach to mechanistic modeling, this work will develop a model for single-chain antibody fragment 4-4-20 (scFv) translocation into and folding within the endoplasmic reticulum (ER) lumen of *Saccharomyces cerevisiae*, or baker's yeast, by the chaperone binding protein (BiP) and foldase protein disulfide isomerase (PDI). The motivation for this study comes from the fact that single-chain antibodies have a variety of applications in biotechnology and medicine (15, 16) and serve as useful models for the expression of other disulfide bond-containing therapeutic proteins. Additionally, yeast is a frequently-used platform, because it combines the ease of microbial genetics and growth characteristics with post-translational, eukaryotic processing (17–19). The goal of using systems biology to study this system is to optimize production of scFv in the *S. cerevisiae* platform.

It has been shown that overexpressing BiP or PDI individually increases scFv yields in the microorganism but overexpressing both simultaneously creates a synergistic effect that amplifies yields over the simple summation of the individual increases alone (17, 20). Xu et al. (20) hypothesized these experimentally-observed BiP and PDI dependencies and synergy originate from BiP assisting in/accelerating unfolded scFv translocation into the ER with no effect on protein folding rates and PDI actually facilitating protein

folding. In this line of reasoning, increasing BiP increases the pool of scFv to be folded, and increasing PDI increases the amount of that pool that is exported from the cell. A mathematical model was developed using the top-down approach to mechanistic modeling to test this hypothesis. Steady-state analysis was employed as a primary analytical method for evaluating model performance. As the top-down approach was applied, its strengths were clearly highlighted as it identified a critical motif and three requirements for successful reproduction of the experimental data.

Model Development Methodology

Establishing Desired Model Behaviors

In implementing the top-down approach, one first identifies the experimental behavior(s) one wishes to capture with the mathematical model. To reiterate, in the case of scFv folding, the model must reproduce the following principal behaviors: scFv expression must be both BiP- and PDI-dependent, and overexpressing BiP and PDI must significantly increase scFv secretion over overexpressing either BiP or PDI alone (i.e., BiP and PDI must display some degree of synergy). These behaviors are captured in a key set of experimental data from Xu et al. (20), reproduced in Figure 2A.

Establishing Desired Model Details

Next, one mines the experimental literature for known and hypothesized interactions and mechanistic details desired for inclusion in the final mechanistic model. In doing so, one establishes the model's scope. Since the scFv

folding model was to be used for evaluating the validity of the Xu et al. (20) hypothesis, it needed to represent the hypothesis's core concepts: BiP assists in unfolded scFv (UscFv) translocation into the ER, and PDI catalyzes protein folding. Other details desired for inclusion in the model were those associated with transcription, translation, and post-translational translocation of the scFv; UscFv, BiP, and PDI binding states; and relative UscFv folding/misfolding rates in each of those binding states. Inclusion of these details would also require three compartments: the nucleus, cytoplasm, and ER.

Constructing a Backbone Model

With the scope of the detailed mechanistic model established, one then identifies the components necessary for construction of a backbone model, the bare minimum that is required for capturing the desired experimental behaviors. This step may be facilitated by searching the catalog of elements (modules, motifs, and interactions) known to be responsible for producing certain biological behaviors for homologies to the system at hand. If one or more plausible matches is/are found, the corresponding element(s) may be applied to the backbone model structure. Experimental validation of the utilization of such elements—notably, combinations thereof in gene regulatory networks—in mathematical model construction to represent and predict biological behavior was performed by Guido et al. (21). If no known modules, motifs, or interactions are appropriate for use in the backbone model, the modeler will have to identify such underlying mechanisms independently.

In the scFv folding example, there was no precedent for the experimentally-

observed scFv folding dependencies, so the latter approach was undertaken. Guidance in constructing a backbone model structure for this system originated from the Xu et al. (20) hypothesis. It was possible to capture this hypothesis most fundamentally in a two-state mathematical model, where unfolded scFv (UscFv) entered the ER in a second-order, BiP-dependent step, and the UscFv folded in preparation for secretion (SscFv) in a second-order, PDI-dependent step. This reaction scheme is illustrated as Model 1 in Figure 3, and its parameters are described and assigned values in Table 2.

When developing a backbone model, enumerating all assumptions and simplifications is an effective means of systematizing the process. If and when a model fails to capture the experimental behaviors, assumptions and simplifications may be altered or relaxed in a methodical fashion. When all of these potential alterations and relaxations have been exhausted, insight gained from the unsuccessful modeling attempt may be applied to the formulation of a new one. The assumptions and simplifications used in construction of the scFv folding backbone model are listed below and explained in the following paragraph.

1. All reactions were modeled using lowest-order, deterministic kinetics.
2. No scFv protein of any form was initially present in the system.
3. Unfolded protein entry to the ER was assumed to have a first-order dependency on BiP.
4. Folding/secretion was assumed to have a first-order dependency on PDI.
5. Pools of 1×10^3 scFv mRNAs, 3.37×10^5 free BiPs, and 5.24×10^5 free PDIs participated in their respective reactions, as described in the reaction equations

and illustrated in Figure 3, and were not consumed.

6. No scFv misfolding or degradation reactions were included.
7. All properly folded scFv was assumed to proceed to the Golgi and ultimately be secreted.

Assumptions (1) and (7) will be common to all mathematical models presented in this paper. The second assumption was meant to mimic the experimental conditions under which the invalidation data were taken, where transfer to galactose-containing medium at time = 0 initiated scFv production. Assumptions (3) and (4) were meant to capture in basic form the central concepts of the Xu et al. (20) hypothesis, and the first-order dependencies arose from assumption (1). Assumption (5) arose from literature-derived values for these concentrations (22–24), and embedded within it was the further, critical assumption that all BiP and PDI was available for reaction with scFv, and none was sequestered away by competing reactions/species. Assumption (6) was made for simplicity, even though it is well documented proteins terminally misfold and are removed from the ER via ER-Associated Degradation (ERAD) (25). Assumption (7) was for pure model simplification reasons. The reaction equations follow. Rate constant values are provided in Table 2, and derivations are provided in the Appendix.

$$\frac{d[\text{UscFv}]}{dt} = k_{1b}[\text{scFvmRNA}][\text{BiP}] - k_{2b}[\text{UscFv}][\text{PDI}] \quad (1)$$

$$\frac{d[\text{SscFv}]}{dt} = k_{2b}[\text{UscFv}][\text{PDI}] \quad (2)$$

All mathematical model simulations in this work were performed using Matlab Simulink using the ode15s solver. Figure 2B, which contains trajectories from the fully-detailed model, exemplifies typical simulation trajectories for all mathematical models from *in silico* runs intended to replicate the Xu et al. (20) experimental results in Figure 2A. All model trajectories displayed the observed linear behavior, so that a concisely effective method for evaluating model performance in replicating the experimental trajectories could be developed by comparing 50 h time point values, as demonstrated in Figure 2C. These values were scaled by the experimental data points to facilitate this simulation-experiment comparison. Error bars from the experimental data point with the *largest* standard deviation (O.PDI at 50 hours) were also included. Model numbers in this Figure correspond to their assignments in Figure 3 and the text, and asterisks indicate models that have been modified with Modification A, which is also schematized in Figure 3.

One benefit of developing a backbone model is it generally facilitates analysis by eliminating the clutter associated with more detailed models. For example, with such a simple model for scFv folding, it was possible to derive analytically the steady-state production of SscFv from the model equations and evaluate its dependencies on BiP and PDI concentrations directly. Steady-state was achieved within the first time step of the simulations, 1×10^3 s, which is consistent with experiments that show pro-scFv (UscFv) reaching steady-state levels within 10 and 60 minutes of the initiation of scFv production. Consequently, this steady-state analysis was appropriate. For this most basic mathematical model, the steady-state SscFv production rate (derived by expressing the SscFv production rate in terms

of system parameters after having set the other states' time dependencies to zero) was:

$$\frac{d[\text{SscFv}]_{SS}}{dt} = k_{1b}[\text{BiP}][\text{mRNA}]. \quad (3)$$

This equation demonstrates that SscFv production was totally independent of PDI levels in this mathematical model. scFv flux through the system was constant and determined at the ER-entry step, modulated by BiP. Increasing/decreasing PDI levels would only decrease/increase, respectively, UscFv levels, but the flux would remain the same. As a result, this model was incapable of reproducing the experimentally-observed scFv folding dependency data where increasing PDI, with or without BiP, increased scFv secretion. Similarly, this first model was unable to demonstrate any kind of synergy between BiP and PDI in SscFv production. These results indicated a fault in the backbone model formulation.

As previously discussed, in a systematic approach to backbone model construction, modifications to the model should be made by systematically altering or relaxing assumptions and simplifications before discarding it completely. Assumption (6) was the first to be altered in the scFv folding model, as it was arguably one of the weakest. This alteration was justified biologically: *in vivo*, if a protein is not successfully folded after some time, it proceeds down the ERAD (ER-Associated Degradation) pathway, where it is retrotranslocated from the ER to cytoplasm and degraded (reviewed in (25)). Hence, protein folding may be viewed as a competition between achieving a properly folded state or a terminally-misfolded state.

To include this detail in the basic, two-state model, a generic degradation pathway was added to the UscFv state, illustrated as the Model 2 in Figure 3. Thus, assumption (6) from the previous model was replaced with the following:

6. UscFv misfolds/degrades in a first order reaction.

and all other assumptions remained the same. The corresponding model equations and the steady-state SscFv production rate follow.

$$\frac{d[\text{UscFv}]}{dt} = k_{1b}[\text{scFvmRNA}][\text{BiP}] - k_{2b}[\text{UscFv}][\text{PDI}] - k_{m5}[\text{UscFv}] \quad (4)$$

$$\frac{d[\text{SscFv}]}{dt} = k_{2b}[\text{UscFv}][\text{PDI}] \quad (5)$$

$$\frac{d[\text{SscFv}]_{SS}}{dt} = \frac{k_{1b}[\text{BiP}][\text{mRNA}][\text{PDI}]}{\frac{k_{m5}}{k_{2b}} + [\text{PDI}]} \quad (6)$$

From the steady-state SscFv production rate, it may be seen that including the degradation pathway also included a PDI dependency, the magnitude of which varies depending on the ratio of the degradation to folding rate constants. The model predicts that as the assisted folding rate constant dominates over degradation, PDI dependence diminishes. For the literature-derived parameter values used in the model (see Appendix for all parameter derivations), there was sufficient PDI dependence to capture both of the two key experimental invalidation behaviors: scFv secretion showed a similar BiP- and PDI-dependency to the experimental measurements (Figure 2C), and BiP and PDI displayed synergy when overexpressing both BiP and PDI increased SscFv levels at 50 h 1.4 times more than the summed

increase in SscFv produced by overexpressing BiP and PDI independently. Based on this significant improvement in model performance resulting from the addition of a degradation pathway, the first in a series of three requirements for the ultimate detailed model to reproduce the experimental data was formulated:

Requirement #1: Competition between degradation/misfolding and accelerated folding by PDI is necessary for PDI dependence.

With the addition of UscFv degradation, a successful backbone model was constructed, and the hypothesized folding process remained viable. Upon formulation of a successful backbone model, the top-down approach to mechanistic modeling proceeds with the gradual supplementation of the model with mechanistic detail until the desired level of detail, defined when the model's scope was being elaborated, has been reached. The order in which these details are added and the quantities added at a time will depend upon the model and its intended use and will consequently require the discretion of the modeler. One consideration to make when proceeding, though, is that one purpose of incrementally appending the model is to enable the modeler to observe and evaluate the discrete effects produced by each alteration. Consequently, it would be desirable to design each increment so as to maximize the insight gained from implementing it. This process is demonstrated with the scFv folding model below.

Further Model Development

For the scFv folding model, further translocation or folding details could not be reasonably added without first including explicit BiP and PDI binding and release of the UscFv. Previously, in Models 1 and 2, the binding and release reactions had been lumped into the second-order reactions for UscFv entry and folding that BiP and PDI, respectively, had catalyzed. Now, it was desired to have BiP bind the UscFv at the translocon for entry to the ER. Upon luminal entry, BiP could theoretically release it, or PDI could also bind the BiP·UscFv complex. It has been hypothesized that PDI is largely incapable of binding unfolded protein on its own in its foldase capacity, and BiP is responsible for making unfolded protein accessible for PDI binding (26), thus increasing the extent to which BiP and PDI cooperate in the protein folding process. The model was later used to assess this hypothesis. UscFv could also transition between the BiP·PDI·UscFv and PDI·UscFv states with the respective release or binding of BiP. True to the top-down modeling approach, these binding states were added incrementally to individually evaluate their effects on the ability of the model to reproduce the experimentally-observed BiP and PDI scFv folding dependencies. The resulting four model permutations are schematized as Models 3-6 in Figure 3. Parameter descriptions and values are provided in Table 2.

With the model constructs established, it was then necessary to assign the folding and misfolding rates associated with each of the binding states. Derivation and references for the actual rate values are presented in the Appendix, but qualitative descriptions and logic are presented here. It is

thought that chaperone proteins such as BiP do not actually promote faster protein folding but rather protect the unfolded protein against misfolding by binding hydrophobic regions (reviewed in (27)). Hence, a BiP-bound unfolded protein would be expected to fold at approximately the same rate as an unbound one, however its effective misfolding rate would be slower than the unbound one. A PDI-bound unfolded protein would be expected to have a faster folding rate but a similar misfolding rate (ignoring PDI's proposed chaperone behavior (28–30), reviewed in (31)) to an unbound one, and a BiP- and PDI- bound unfolded protein would be expected to have both a faster folding rate *and* a slower misfolding rate. Assumptions and simplifications for the four model permutations follow:

1. All reactions were modeled using lowest-order, deterministic kinetics.
2. No scFv protein of any form was initially present in the system.
3. Unfolded protein entry to the ER was assumed to have a first-order dependency on BiP.
4. Folding/secretion was assumed be first-order and faster for BiP-PDI-bound and PDI-bound than BiP-bound and unbound UscFv.
5. A pool of 1×10^3 scFv mRNAs participated in the luminal UscFv production reaction but was not consumed.
6. 3.37×10^5 free BiPs and 5.24×10^5 free PDIs were available for UscFv binding and were consumed in the binding reactions and regenerated upon release.
7. All properly folded scFv was assumed to proceed to the Golgi and ultimately be secreted.
8. Misfolding/degradation was assumed be first-order and equivalent for both BiP-PDI-bound BiP-bound UscFv but faster for both unbound and PDI-bound UscFv.
9. BiP binding was required for PDI binding to occur.

10. Multiple binding by BiP and PDI was ignored for simplicity, and folding/misfolding rates were based on overall folding/misfolding rates, as derived in the Appendix.

Due to the increasing size and number of models, their ODEs have been relegated to the Appendix, though it must be noted that the initial step of importing UscFv to the ER/BiP·UscFv production term was always represented by $k_1[\text{BiP}][\text{scFv mRNA}]$ in the BiP·UscFv equations. Analytical solutions for the model permutations' steady-state SscFv production rates are presented below (Model 3: Equation 7; Model 4: Equation 8; Model 5: Equation 9; and Model 6: Equation 10). In deriving these solutions, a further assumption was employed in order to make the algebra tenable: unbound BiP and PDI were sufficiently abundant over UscFv, so their concentrations were not altered by binding UscFv. This assumption held during simulations, where BiP and PDI concentrations remained 3.37×10^5 and 5.24×10^5 molecules, respectively, while bound species never exceeded 100 molecules.

$$\frac{d[\text{SscFv}]_{SS}}{dt} = \frac{k_1[\text{BiP}][\text{scFv mRNA}](k_3(k_{r2} + k_4 + k_{m4}) + k_2[\text{PDI}]k_4)}{(k_3 + k_{m3})(k_{r2} + k_4 + k_{m4}) + k_2[\text{PDI}](k_4 + k_{m4})} \quad (7)$$

$$\frac{d[\text{SscFv}]_{SS}}{dt} = \frac{k_1[\text{BiP}][\text{scFv mRNA}](k_3 + \frac{k_4 k_2 [\text{PDI}]}{k_{r2} + k_4 + k_{m4}} + \frac{k_7 k_{r6}}{k_6[\text{BiP}] + k_7 + k_{m7}})}{k_{r6} \left(1 - \frac{k_6[\text{BiP}]}{k_6[\text{BiP}] + k_7 + k_{m7}}\right) + k_2[\text{PDI}] \left(1 - \frac{k_{r2}}{k_{r2} + k_4 + k_{m4}}\right) + k_3 + k_{m3}} \quad (8)$$

$$\begin{aligned} \frac{d[\text{SscFv}]_{SS}}{dt} &= \frac{k_3 k_1 [\text{BiP}][\text{scFv mRNA}]}{k_2[\text{PDI}] + k_3 + k_{m3}} + \\ &\quad \frac{k_3 k_{r2}}{k_2[\text{PDI}] + k_3 + k_{m3}} + k_4 + \frac{k_5 k_{r6}}{k_6[\text{BiP}] + k_5 + k_{m5}} \cdot \\ &\quad \left\{ \frac{k_1[\text{BiP}][\text{scFv mRNA}]k_2[\text{PDI}]}{(k_2[\text{PDI}] + k_3 + k_{m3}) \left(1 - \frac{k_6[\text{BiP}]}{k_6[\text{BiP}] + k_5 + k_{m5}}\right) + k_{r2} \left(1 - \frac{k_2[\text{PDI}]}{k_2[\text{PDI}] + k_3 + k_{m3}}\right)} \right\} \quad (9) \end{aligned}$$

$$\begin{aligned} \frac{d[\text{SscFv}]_{SS}}{dt} &= \left\{ k_3 + \frac{k_2[\text{PDI}]}{k_{r2} + k_{r6} \left(1 - \frac{k_6[\text{BiP}]}{k_6[\text{BiP}] + k_5 + k_{m5}}\right) + k_4 + k_{m4}} \cdot \right. \\ &\quad \left. k_4 + \frac{k_5 k_{r6}}{k_6[\text{BiP}] + k_5 + k_{m5}} + \frac{k_7 k_{r6}}{k_6[\text{BiP}] + k_7 + k_{m7}} \right\} \cdot \\ &\quad \left\{ \frac{k_1[\text{BiP}][\text{scFv mRNA}]}{k_{r6} \left(1 - \frac{k_6[\text{BiP}]}{k_6[\text{BiP}] + k_7 + k_{m7}}\right) + k_2[\text{PDI}] \left(1 - \frac{k_{r2}}{k_{r2} + k_{r6} \left(1 - \frac{k_6[\text{BiP}]}{k_6[\text{BiP}] + k_5 + k_{m5}}\right) + k_4 + k_{m4}}\right)} \right\} + k_3 + k_{m3} \quad (10) \end{aligned}$$

As may be observed in these equations, the aforementioned BiP·UscFv production term, $k_1[\text{BiP}][\text{scFv mRNA}]$, appears in the numerator in each of the model permutations' expression for steady-state SscFv production, indicating production in each permutation was largely linearly dependent on BiP concentration. On the other hand, production dependence on PDI concentration assumed a Michaelis-Menton-like form. The linear BiP dependence overpowered PDI's contribution for a range of BiP and PDI concentrations (not shown), so in order to reproduce the experimental data, it was necessary to overexpress PDI an order of magnitude times more than BiP (Figure 2C, Table 1). To modify this behavior, the assumptions and simplifications that went into deriving the models were re-evaluated for alterations.

The approach was to identify the mechanistic origins for the BiP and PDI dependencies observed in the steady-state production terms. BiP’s role in translocation of the UscFv into the ER dominated over any other contribution it made in the folding process, and since the translocation reaction was a second-order, bimolecular reaction between BiP and mRNA, BiP dependency was linear. From the backbone model development, it was observed that including a degradation pathway to compete with a species-dependent pathway instilled a Michaelis-Menton-like dependence on that species’ (i.e., PDI’s) concentration in the steady-state SscFv production rate expression. This branched dependency-degradation competition motif could then potentially be applied to BiP’s role in translocation, so steady-state SscFv production would have a Michaelis-Menton-like dependence on both BiP and PDI. Since BiP “catalyzing” translocation of UscFv into the ER was the dependency step, it needed to compete with a degradation step, such as cytoplasmic UscFv degradation, for the motif to be complete. A schematic representation of this modification is presented in Figure 3 (Modification A); it is shown implemented in Model 8; and Models 3-6 with this modification will be denoted with an asterisk as Models 3*-6*. This theoretical alteration translated into the alteration of assumption (5), whose revised version appears below:

5. scFv transcription was modeled by a step input of cytoplasmic UscFv that could be consumed by cytoplasmic degradation and translocation into the ER to yield 1×10^3 scFv mRNA during steady-state SscFv production.

The fully modified differential equations for each model permutation appear in the Appendix; however, it is instructive to analyze the differ-

ential equation for cytoplasmic UscFv production—common to all model permutations—which resulted from the revised assumption (5):

$$\frac{d[\text{cytoplasmic UscFv}]}{dt} = V_{UscFv} - k_1[\text{BiP}][\text{cytoplasmic UscFv}] - k_d[\text{cytoplasmic UscFv}]. \quad (11)$$

When this equation is analyzed at the steady state,

$$[\text{cytoplasmicUscFv}] = \frac{V_{UscFv}}{k_1[\text{BiP}] + k_d}, \quad (12)$$

a steady-state BiP·UscFv production term (i.e., the BiP-dependent translocation rate) for the altered models may be derived: $\frac{V_{UscFv}k_1[\text{BiP}]}{k_1[\text{BiP}] + k_d}$. This term, with its distinct Michaelis-Menton-like dependence on BiP, supplants $k_1[\text{BiP}][\text{scFv mRNA}]$ in the previous models' expressions for steady-state SscFv production (Equations 7-8), so that both BiP and PDI have similar concentration dependencies. The similar steady-state BiP and PDI SscFv production value dependencies shown in Figure 4 and the comparable BiP and PDI relative overexpression levels required to reproduce the experimentally-observed BiP and PDI dependencies in Figure 2C provided in Table 1 reinforce this result with simulation data. At this point, a second requirement is claimed:

Requirement #2: Assuming post-translational translocation is BiP-dependent, cytoplasmic degradation of unfolded scFv is required to make BiP and PDI expression level dependencies comparable.

Besides identifying a second requirement for a detailed scFv folding model to reproduce experimentally-observed BiP and PDI dependencies, the top-down approach to mechanistic modeling has also identified an important biological structural motif. A degradative pathway competing with a species-dependent pathway results in a Michaelis-Menton-like dependency on that species by a downstream product. This branched dependency-degradation competition motif may then be added to the catalog of known biological motifs and modules responsible for producing certain biological behaviors for future model building.

It may also be noted that another way to introduce a branched dependency-degradation competition motif for BiP in the scFv folding model—alluded to in the statement of Requirement #2—is by eliminating BiP’s participation in post-translational translocation of the UscFv to the ER (Model 7 in Figure 3). In this case, UscFv enters the ER unbound, where it may “degrade” by folding or misfolding (degradation branch of the motif) before being reversibly bound by BiP (dependency branch). The steady-state BiP·UscFv production term in this case, $\frac{k_6[\text{BiP}](k_1[\text{scFv mRNA}] + k_{r6}[\text{BiP}\cdot\text{U}])}{k_6[\text{BiP}] + k_7 + k_{m7}}$, demonstrates this Michaelis-Menton-like dependency, so that the expression for steady-state SscFv production thus shows such a dependence on both BiP and PDI:

$$\frac{d[\text{SscFv}_{SS}]}{dt} = \frac{k_7 k_1 [\text{scFv mRNA}]}{k_6 [\text{BiP}] + k_7 + k_{m7}} + \frac{k_7 k_{r6}}{k_6 [\text{BiP}] + k_7 + k_{m7}} + k_3 + \frac{k_4 k_2 [\text{PDI}]}{k_{r2} + k_4 + k_{m4}} \cdot \left\{ \frac{k_6 k_1 [\text{BiP}] [\text{scFv mRNA}]}{(k_6 [\text{BiP}] + k_7 + k_{m7}) \left(1 - \frac{k_{r6}}{k_6 [\text{BiP}] + k_7 + k_{m7}} + k_2 [\text{PDI}] \left(1 - \frac{k_{r2}}{k_{r2} + k_4 + k_{m4}} + k_3 + k_{m3} \right) \right)} \right\}. \quad (13)$$

From this result, one may conclude that the Xu et al. (20) hypothesis is not exclusive in possessing the ability to reproduce experimentally-observed BiP and PDI dependencies in scFv folding, though the BiP-independent translocation model is inconsistent with experimental evidence of BiP-scFv associations (32).

In returning to the hypothesis-based model development, there were four permutations of the model iteration that included explicit BiP and PDI binding details that were capable, to some extent, of capturing the experimentally-observed BiP and PDI dependencies. Before developing a means to distinguish between these models in another capacity, one final permutation was established to evaluate the hypothesis that PDI requires BiP-bound UscFv for binding as a foldase, as previously described. This final permutation's performance, which represents the alternative case where PDI may bind UscFv directly (Model 8 in Figure 3; note that this model already has Modification A implemented in it), would be evaluated in the same capacity as the other permutations.

While the analytical solution for steady-state SscFv production in this final model permutation is fairly complex (see Appendix), it does exhibit Michaelis-Menton-like dependencies on both BiP and PDI. Additionally, the BiP and PDI dependency plots demonstrated little deviation from the other permutations in its ability to reproduce the experimental data (Figure 2C). Consequently, it may be concluded that the branched dependency-degradation competition motifs for BiP and PDI, whose mechanistic bases are described in Requirements #s 1 and 2, are solely responsible for instill-

ing a mathematical model at this level of detail with the ability to capture experimentally-observed BiP and PDI dependencies, and the hypothesized passage of UscFv to PDI through BiP is not.

Up to now, focus has been placed on evaluating the model permutations' ability to reproduce BiP and PDI dependencies. The other key experimental behavior desired for a successful mathematical model to exhibit was synergy between BiP and PDI in producing SscFv. To evaluate the synergy displayed by each of the five model permutations, the steady-state rate of SscFv production when both BiP and PDI were overexpressed—normalized by the production rate with nominal BiP and PDI levels—was divided by the sum of the normalized SscFv production rates when BiP and PDI were overexpressed individually, for multiple BiP and PDI overexpression levels (Figure 5). The Figure plots the calculated synergies for BiP and PDI overexpression levels of the same relative amounts (e.g., both BiP and PDI were overexpressed 10-fold, 20-fold, etc.), though similar trends were observed for all other calculated permutations in BiP and PDI levels in the 10- to 100-fold overexpression range (e.g., BiP overexpressed 10-fold and PDI overexpressed 20-fold, BiP overexpressed 20-fold and PDI overexpressed 10-fold, etc.). All of the models displayed a similar degree of synergy within this overexpression range, about half the same value calculated and averaged for all time points in the Xu et al. (20) et al data (2.2 ± 0.7 ; not on plot). Consequently, between being able to reproduce experimentally-observed BiP and PDI overexpression dependencies and synergy, all model permutations appeared to be similarly valid, so that any protein folding model would not be unique in its ability to represent the scFv folding system.

At this stage of model development, there was one final issue to be addressed pertaining to the biological validity of assumption 6.: 3.37×10^5 free BiPs and 5.24×10^5 free PDIs were available for UscFv binding and were consumed in the binding reactions and regenerated upon release. BiP has many roles in the ER (most reviewed in (27); karyogomy function described in (33)) and, consequently, interacts with many proteins there, and PDI accelerates the folding of any disulfide bond-containing species. To better represent this biological sequestration of BiP and PDI from UscFv, a pool of total (non-scFv) unfolded protein was introduced to which BiP and PDI could bind. This modification is schematized as Modification B in Figure 3. Upon implementation of Modification B, one also introduces a useful means of tuning SscFv production rates.

That is, as available BiP and PDI levels are altered through introduction of this pool of generic unfolded protein, SscFv production dependencies are also altered per the BiP and PDI dependency curves in Figure 4, as long as free BiP and PDI are available in excess (the assumption under which the dependency curves were generated). If either BiP or PDI concentrations approach and fall below UscFv levels, SscFv production dependence will be dominated by the limiting species-behavior that is not captured by the curves. To control the amount of BiP and PDI sequestered away by generic unfolded protein, the amount of generic unfolded protein present and/or BiP and PDI's affinities for unfolded protein may be altered. In this work, the amount of generic unfolded protein was kept constant at 1.5×10^5 , while the affinities were altered, so that an excess of 1.87×10^5 unbound BiP and 3.74×10^5 unbound PDI remained at steady state.

Completion of the Fully-Detailed Model

Even though all model permutations containing explicit BiP and PDI binding were similarly capable of capturing desired BiP and PDI dependencies and synergistic behavior, Model 6* was selected for further development, because its mechanistic structure most resembled the desired fully-detailed model structure. In transforming Model 6* to the fully-detailed model, details pertaining to scFv transcription and translation and an extra step to the post-translational translocation process were added (Figure 6) with no effect on model performance with regards to capturing BiP and PDI dependencies (Figure 2C) and synergy (not shown). The list of model assumptions and simplifications for the fully-detailed model follows. System ODEs are included in the Appendix. Parameters, some of which were renamed from the simpler models, are listed in Table 2.

1. All reactions were modeled using lowest-order, deterministic kinetics.
2. No scFv transcript or protein of any form was initially present in the system.
3. BiP binds UscFv at the translocon in a second-order reaction, and UscFv enters in a first-order reaction step.
4. Folding/secretion was assumed be first-order and faster for BiP-PDI-bound and PDI-bound than BiP-bound and unbound UscFv.
5. scFv transcription was a step input.
6. 3.37×10^5 total BiP and 5.24×10^5 total PDI were available for UscFv and general unfolded protein binding and were consumed in the binding reactions and regenerated upon release.
7. All properly folded scFv was assumed to proceed to the Golgi and ultimately be secreted.

8. Misfolding/degradation was assumed be first-order and equivalent for both BiP-PDI-bound BiP-bound UscFv but faster for both unbound and PDI-bound UscFv.
9. BiP binding was required for PDI binding to occur.
10. Multiple binding by BiP and PDI was ignored for simplicity, and folding/misfolding rates were based on overall folding/misfolding rates, as derived in the Appendix.

Results

Having developed a detailed mechanistic model using the top-down approach, analysis could proceed. The model development process does not affect the applicability of available analytical methods, reviewed in (10), as mentioned in the Introduction, though they may be applied more efficiently and effectively when the top-down approach is used due to the insights one has attained in incrementally constructing the model. In the case of the scFv folding model, the insights gained in model development guided the prediction and evaluation of parameter dependencies of SscFv production.

Development of the backbone model for scFv folding identified the core processes required for reproduction of experimental behaviors. These were translocation by BiP and branched folding by PDI that competed with degradation. All subsequently-added supplemental details elaborated these basic processes. Consequently, predictions could be made for large groups of parameters within these processes as to how they would affect SscFv production.

Starting with the PDI folding/degradation competition process, it would follow that changes in parameters associated with folding would similarly affect SscFv production, and changes in parameters associated with mis-

folding would inversely affect production. Thus, increasing folding rates and decreasing misfolding rates would be expected to increase SscFv production. Additionally, adjusting BiP- and PDI-UscFv binding/dissociation rates so as to increase the production of the fastest folding, slowest misfolding UscFv binding state (BiP·PDI·UscFv) over slower folding and faster misfolding states would also increase SscFv production. Indeed, these predictions were verified when the parameter alterations were implemented in the mathematical model (Figure 7, which shows the relative SscFv dependencies to the various folding, misfolding, binding, and dissociation rates). Relative overall misfolded scFv production dependencies were simply the inverse of these results (not shown).

Similar predictions and verifications could be performed for parameter dependencies in the BiP translocation process. In a logical fashion, it could be anticipated that increases/decreases in parameters associated with transcription and translation would result in increased/decreased SscFv production (verification not shown). However, there was one parameter that proved to be critical to model performance: the rate at which the translocation complex formed, which included UscFv trafficking to the translocon and BiP binding to it in a second-order reaction. Reasoning would predict that low values of this parameter would limit the translocation process, so SscFv production would be highly BiP dependent. High values of this parameter would flood the ER with UscFv, so SscFv production would become folding—hence, PDI—limited. Consequently, this parameter could potentially dictate relative SscFv dependencies to BiP and PDI levels.

To verify this prediction, SscFv levels at 50 h were plotted against the

experimental measurements for a range of translocation complex formation rates for various BiP and PDI overexpression levels, as shown in Figure 8. In the plots, it may be observed that, indeed, there is a gradual transition from total BiP dependence to total PDI dependence by SscFv production as the translocation rate increases. It is only within an intermediate range, around $2.2 \times 10^{-9} \frac{1}{\text{molecules}\cdot\text{s}}$, that BiP and PDI dependencies are comparable. (The literature-derived value, $1.2 \times 10^{-8} \frac{1}{\text{molecules}\cdot\text{s}}$, used in model development falls within this range.) Since the value of this parameter is so critical for reproducing experimentally-observed BiP and PDI dependencies, it becomes one final model requirement:

Requirement #3: The rate constant associated with the second-order BiP-dependent reaction step in translocation must not be so low compared to PDI-dependent folding rates that it excessively amplifies BiP over PDI expression level dependency. It also should not be so high that it eliminates BiP dependency altogether and makes the system PDI folding-dependent.

Conclusions

In this work, a top-down approach to mechanistic modeling was presented and its implementation demonstrated through the development of a mathematical model for scFv folding in *S. cerevisiae* ER by BiP and PDI. This approach, represented schematically in Figure 1, may be literally summarized with the following steps:

1. Establish the training data, or experimental data the mathematical model is ex-

pected to reproduce.

2. Establish the scope of the model, or the biological details the model will include.
3. Develop and analyze a backbone model, the most basic abstraction of the biological system that can reproduce the desired biological behaviors, potentially from known biological behavior motifs.
4. Incrementally append the backbone model with desired biological details and evaluate their effects on model performance until the desired level of mechanistic detail has been achieved.

As part of the model development, the importance of annotating all assumptions and simplifications was emphasized, as systematic alteration and relaxation of these assumptions and simplifications could be used to conclusively eliminate poorly performing model formulations.

When it was employed to develop a mechanistic mathematical model for scFv folding based on the Xu et al. (20) hypothesis, the strength of the top-down approach was demonstrated as it identified three requirements and a biological behavior motif necessary to reproduce experimentally-observed BiP and PDI dependencies and synergy in scFv folding, thus supporting the hypothesis. Elucidation of these requirements and motif, which naturally arose as part of the top-down process, would not have been so straightforward had a bottom-up—where all mechanistic details are included at once to start—approach been implemented. The requirements are reiterated below:

Requirement #1: Competition between degradation/misfolding and accelerated folding by PDI is necessary for PDI dependence.

Requirement #2: Assuming post-translational translocation is BiP-dependent, cytoplasmic degradation of unfolded scFv is required

to make BiP and PDI expression level dependencies comparable.

Requirement #3: The rate constant associated with the second-order BiP-dependent reaction step in translocation must not be so low compared to PDI-dependent folding rates that it excessively amplifies BiP over PDI expression level dependency. It also should not be so high that it eliminates BiP dependency altogether and makes the system PDI folding-dependent.

The field of systems biology is only recently emerging as a viable means for studying biological systems thanks to recent advances in experimental data gathering and analysis techniques and tools (34). As the field continues to develop and become more standardized, a systematization of the approaches to mathematical modeling of biological systems will assist in this standardization. As these approaches are systematized, formal comparisons and evaluations of their appropriateness and performance for use in modeling particular systems will most certainly arise.

It is even possible that, eventually, certain aspects of modeling approach selection and implementation will be automated. Already, much effort is being placed into developing literature and database mining algorithms and software (35–39) to enumerate experimentally-observed species interactions and define model scope. Upon the eventual creation of a formal biological behavior motifs database, algorithms and software could also be developed to mine it for motifs for use in backbone model construction in the top-down approach to mechanistic modeling. Also specific to the top-down approach, the process of appending the backbone model with further mechanistic de-

tail and analyzing the effects could be automated to a certain extent, similar to the manner in which model reduction continues to be with the bottom-up approach (40–44). Indeed, this work takes only an initial step into systematized mechanistic biological modeling, with much work yet to be done.

Figure Legends

Figure 1.

Overview of the top-down approach to mechanistic biological modeling methodology presented in this work. Inputs and outputs to the methodology are indicated with dotted arrows; methodology flow is indicated by solid arrows.

Figure 2.

A. Experimental scFv secretion data reproduced from Xu et al. (20). “O.” refers to “overexpressed.” Overexpression levels are provided in the reference. B. *In silico* reproduction of this data, using the fully-detailed mathematical model. C. 50 h time points for all model simulations normalized to the respective 50 h experimental time points in Figure 2A (e.g., the 50 h O.BiP model time points are divided by the experimental 50 h O.BiP data point). The similarly-scaled experimental 50 h time points to which this data is compared are represented by the horizontal dashed magenta line of value one. Thus, models that have normalized 50 h time points close to one for all BiP and PDI expression levels are most successful at reproducing the experimental data. Scaled error bars for the experimental 50 h data point with the *highest* standard deviation (0.2 relative units for O.PDI) are provided on the plot (O.BiP and O.BiP+PDI had standard deviations of 0.05 relative units). BiP and PDI overexpression levels used to produce this plot are provided in Table 1.

Table 1.

Table 1: BiP and PDI overexpression levels used in *in silico* experiments to produce the data found in Figure 2.

<i>Model</i>	1	2	3	3*	4	4*	5	5*	6	6*	7	8	Detailed
<i>BiP Overexpression</i>	2×	1.5×	1.5×	40×	1.5×	40×	1.5×	20×	2×	40×	3×	100×	2×
<i>PDI Overexpression</i>	2×	2×	10×	40×	10×	40×	10×	80×	10×	40×	20×	15×	4×

Figure 3.

Schematics for all models, except for the fully-detailed model, and model modifications. Models 1 and 2 were used in backbone model development. Models 3-6 represent the original four permutations of models containing explicit BiP and PDI binding and release. When Modification A was applied to these models, they were designated Models 3*-6*, which are not schematized here. Model 7 represents a binding permutation model where the branched dependency-degradation competition motif for BiP was introduced by eliminating BiP's role in post-translational translocation. Model 8 depicts a final permutation where UscFv may freely move between BiP and PDI binding states and has Modification A implemented in it.

Table 2.

Table 2: Parameters definitions, values, and references.

<i>Developing Models Parameter</i>	<i>Detailed Model Parameters</i>	<i>Definition</i>	<i>Value</i>	<i>Units</i>	<i>Reference(s)</i>
k_1	N/A	Effective second-order rate constant for scFv translation and translocation into the ER by bound BiP	1.2×10^{-8}	$\frac{1}{\text{molecules}\cdot\text{s}}$	(23, 45, 46)
k_{1b}	N/A	Effective second-order rate constant for scFv translation and BiP-catalyzed translocation into the ER	1.2×10^{-8}	$\frac{1}{\text{molecules}\cdot\text{s}}$	(23, 45, 46)
k_{1bit}	N/A	Effective first-order rate constant for scFv translation and BiP-independent translocation into the ER	4.0×10^{-3}	$\frac{1}{\text{s}}$	(23, 45, 46)
k_2	k_{61}	PDI-UscFv binding rate	2.3×10^{-7}	$\frac{1}{\text{molecules}\cdot\text{s}}$	(47-49)
k_{2b}	N/A	PDI-catalyzed UscFv folding rate	1.6×10^{-7}	$\frac{1}{\text{molecules}\cdot\text{s}}$	(26, 47-51)
k_{r2}	k_{r61}	PDI-UscFv release rate	6.0×10^{-4}	$\frac{1}{\text{s}}$	(47-49)
k_3	k_{63}	BiP-UscFv folding rate	7.0×10^{-3}	$\frac{1}{\text{s}}$	(26, 50, 51)
k_d	k_{3d}	Cytoplasmic scFv mRNA degradation rate	2.6×10^{-3}	$\frac{1}{\text{s}}$	(52)
k_{m3}	k_{m63}	BiP-UscFv misfolding rate	3.9×10^{-2}	$\frac{1}{\text{s}}$	(26, 50, 51)
k_4	k_{65}	BiP-PDI-UscFv folding rate	3.4	$\frac{1}{\text{s}}$	(26, 50, 51)
k_{m4}	k_{m65}	BiP-PDI-UscFv misfolding rate	3.9×10^{-2}	$\frac{1}{\text{s}}$	(26, 50, 51)
k_5	k_{66}	PDI-UscFv folding rate	8.5×10^{-2}	$\frac{1}{\text{s}}$	(26, 50, 51)
k_{m5}	k_{m66}	PDI-UscFv misfolding rate	3.4×10^{-1}	$\frac{1}{\text{s}}$	(26, 50, 51)
k_6	k_{60}	BiP-UscFv binding rate	1.2×10^{-8}	$\frac{1}{\text{molecules}\cdot\text{s}}$	(45)
k_{r6}	k_{r60}	BiP-UscFv release rate	1.0×10^{-1}	$\frac{1}{\text{s}}$	(45, 53)
k_7	k_{64}	UscFv folding rate	7.0×10^{-3}	$\frac{1}{\text{s}}$	(26, 50, 51)
k_{m7}	k_{m64}	UscFv misfolding rate	3.4×10^{-1}	$\frac{1}{\text{s}}$	(26, 50, 51)
N/A	k_{55}	scFv mRNA nuclear translocation rate	1.8	$\frac{1}{\text{s}}$	(54-60)
N/A	k_{56}	scFv translation rate	6.2×10^{-2}	$\frac{1}{\text{s}}$	(61, 62)
N/A	k_{58}	UscFv trafficking rate to the translocon	2.2×10^{-9}	$\frac{1}{\text{molecules}\cdot\text{s}}$	(63)
N/A	k_{59}	UscFv posttranslational translocation rate	9.0×10^{-1}	$\frac{1}{\text{s}}$	(46)
N/A	k_{69}	BiP-unfolded protein binding rate	8.8×10^{-2}	$\frac{1}{\text{molecules}\cdot\text{s}}$	(64)
N/A	k_{r69}	BiP-unfolded protein release rate	1.0×10^{-1}	$\frac{1}{\text{s}}$	(64)
N/A	k_{70}	PDI-unfolded protein binding rate	2.3×10^{-7}	$\frac{1}{\text{molecules}\cdot\text{s}}$	(47-49)
N/A	k_{r70}	PDI-unfolded protein release rate	6.0×10^{-4}	$\frac{1}{\text{s}}$	(47-49)
N/A	k_{76}	PDI-unfolded protein binding rate as a chaperone	2.3×10^{-7}	$\frac{1}{\text{molecules}\cdot\text{s}}$	(47-49)
N/A	k_{r76}	PDI-unfolded protein release rate as a chaperone	3.2×10^{-1}	$\frac{1}{\text{s}}$	(31, 47-49)
N/A	k_{57}	Cytoplasmic UscFv degradation rate	4.0×10^{-4}	$\frac{1}{\text{s}}$	(65)

Figure 4.

Curves depicting the Michaelis-Menton-like dependencies of steady-state Ss-cFv production on BiP (A.) and PDI (B.) levels for Models 3*-6* and 8.

Figure 5.

Curves depicting the relative rate of steady-state SscFv production when BiP and PDI are overexpressed (“O.BiP+PDI”) compared to the sum of the production when BiP and PDI are overexpressed independently (“O.BiP+O.PDI”)

for a variety of BiP and PDI overexpression levels for Models 3*-6* and 8. In this plot, “Relative BiP and PDI” indicates the factor by which both BiP and PDI were overexpressed for that particular value. Values for further permutations in relative BiP and PDI overexpression were calculated, but they displayed similar relative behavior and are not included on this plot for simplicity. SscFv levels used in the calculations were normalized by the nominal value obtained with no BiP nor PDI overexpression.

Figure 6.

Schematic for the fully-detailed scFv folding model. State numbers are provided for comparison with equations in the code. Parameter values are provided in Table 2.

Figure 7.

Relative SscFv production dependency on UscFv folding and misfolding and BiP- and PDI-UscFv binding/release rate parameters, as defined in Table 2 and depicted in Figure 6. Generally, parameter numbers with a corresponding “r” are binding rates, and the “r” rates are dissociation rates; parameter numbers with a corresponding “m” are folding rates, and the “m” rates are misfolding rates. SscFv levels were measured at 50 h.

Figure 8.

Plots demonstrating SscFv production dependency on the rate at which cytoplasmic UscFv was trafficked to the translocon (k_{58}) for double BiP and PDI (A.), triple BiP and PDI (B.), and quadruple BiP and PDI (C.)

overexpression levels. SscFv levels were measured at 50 h and compared to the experimental values (dashed lines). Error bars for the experimental data are provided on one experimental data point for ease of interpretation but apply to all: O.BiP+PDI and O.BiP error bars are found at $k_{58} = 1.2 \times 10^{-9} \frac{1}{\text{molecules}\cdot\text{s}}$; O.PDI, at $2.2 \times 10^{-9} \frac{1}{\text{molecules}\cdot\text{s}}$; and nominal, at $3.2 \times 10^{-9} \frac{1}{\text{molecules}\cdot\text{s}}$.

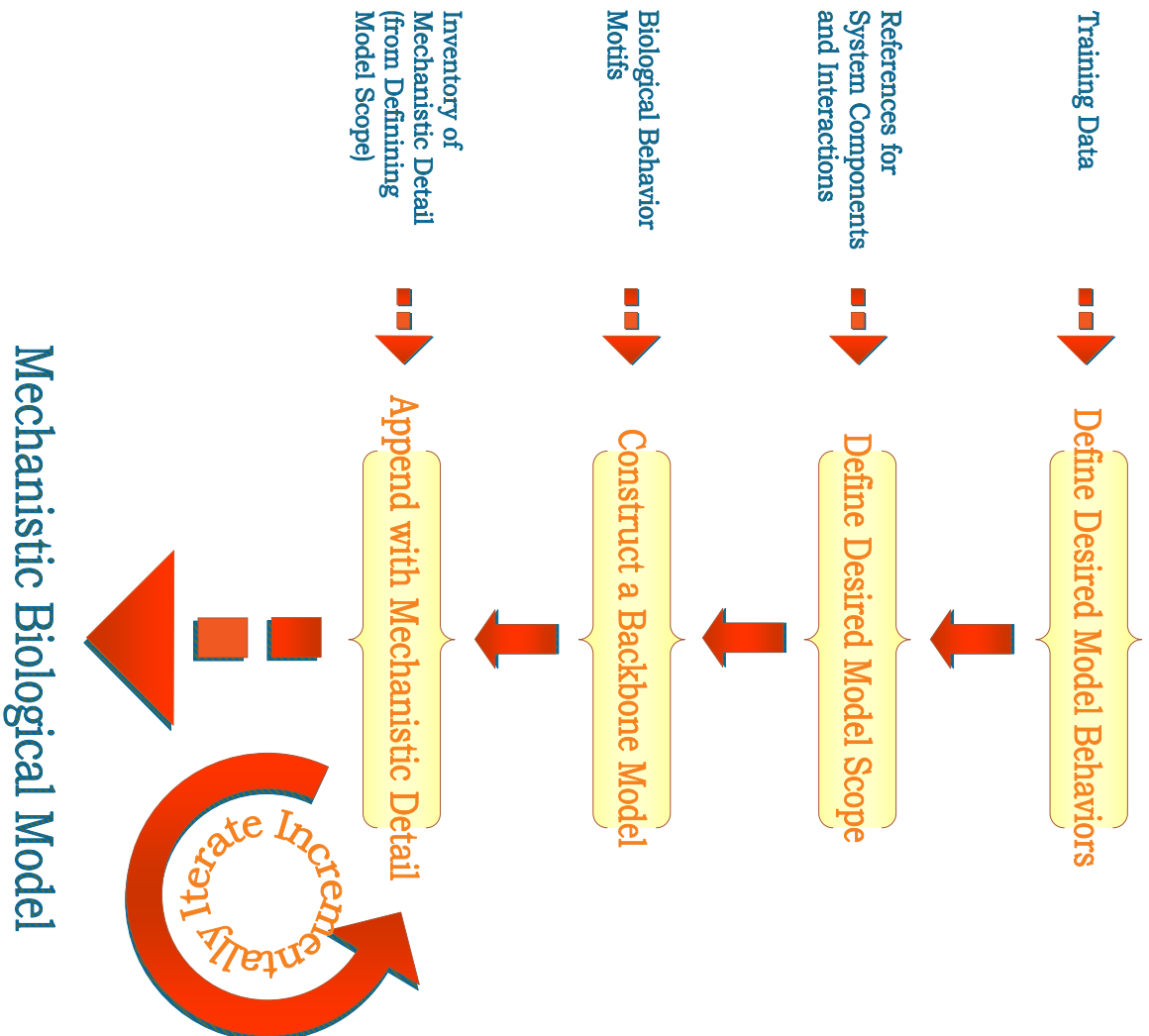


Figure 1:

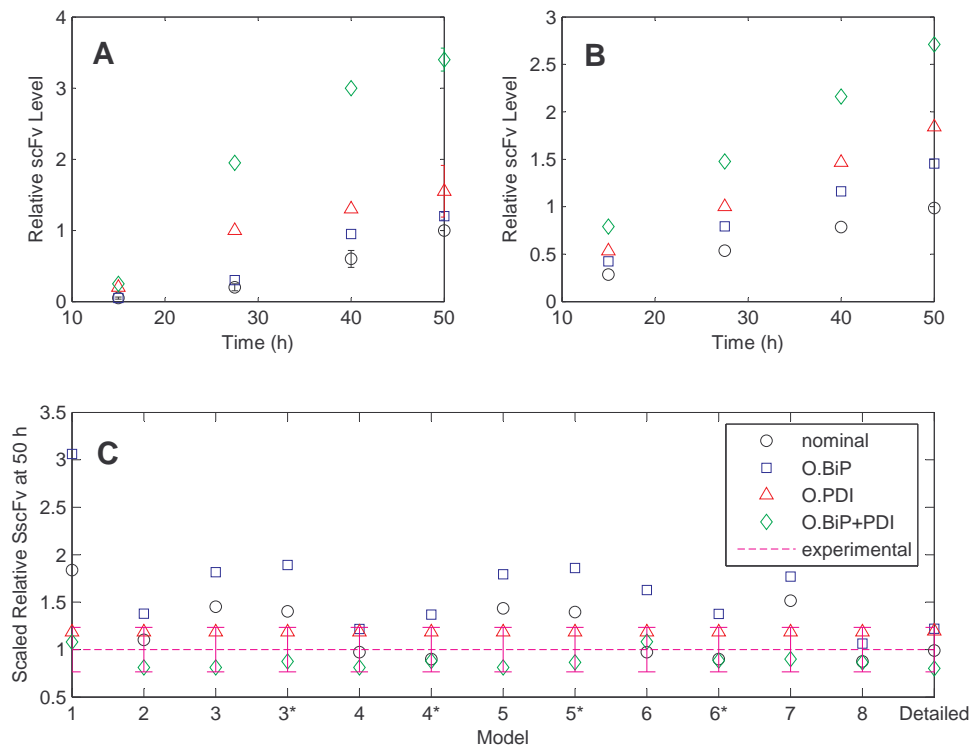


Figure 2:

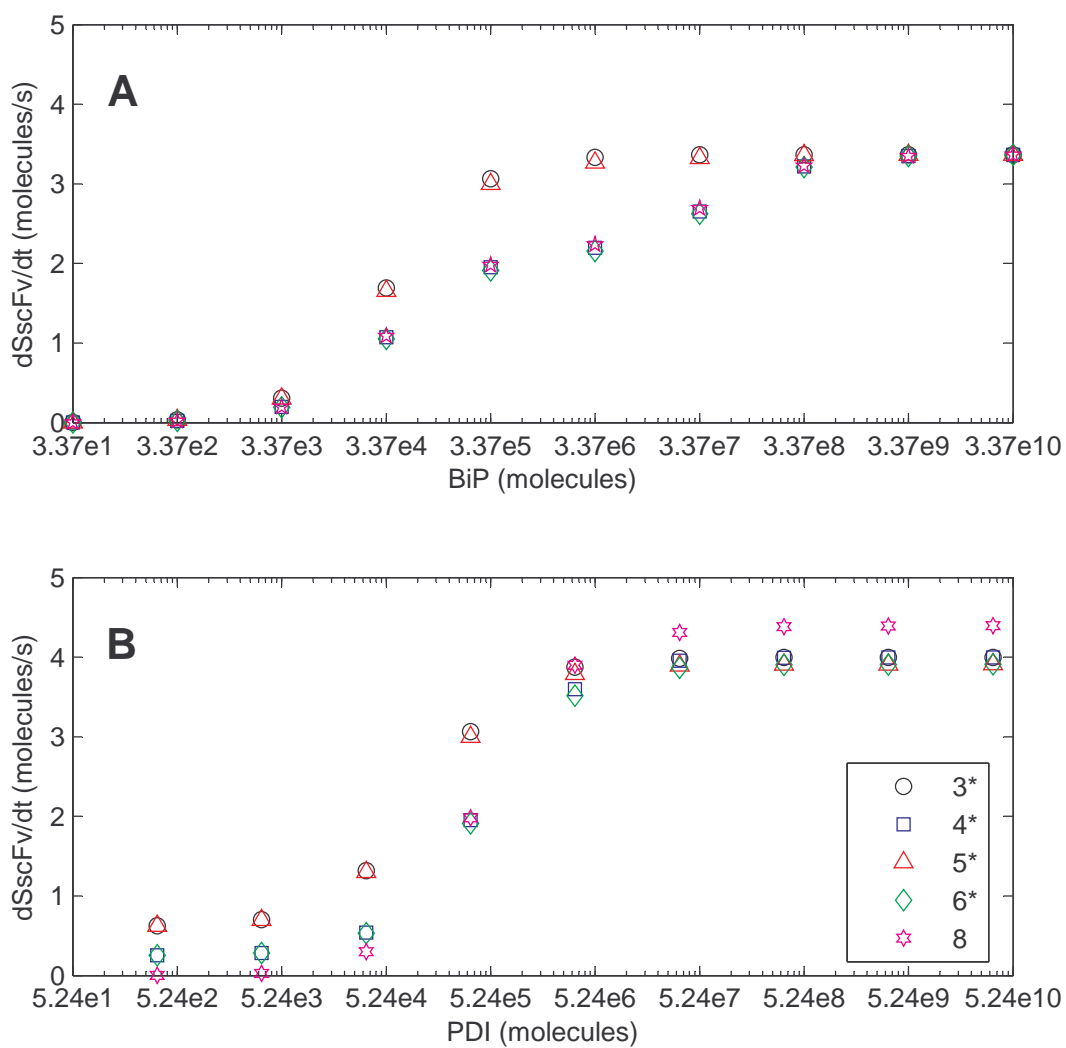


Figure 4:

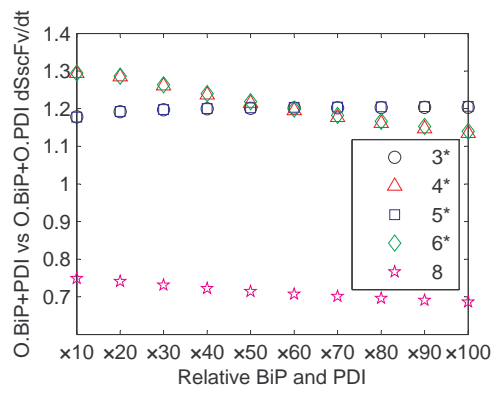


Figure 5:

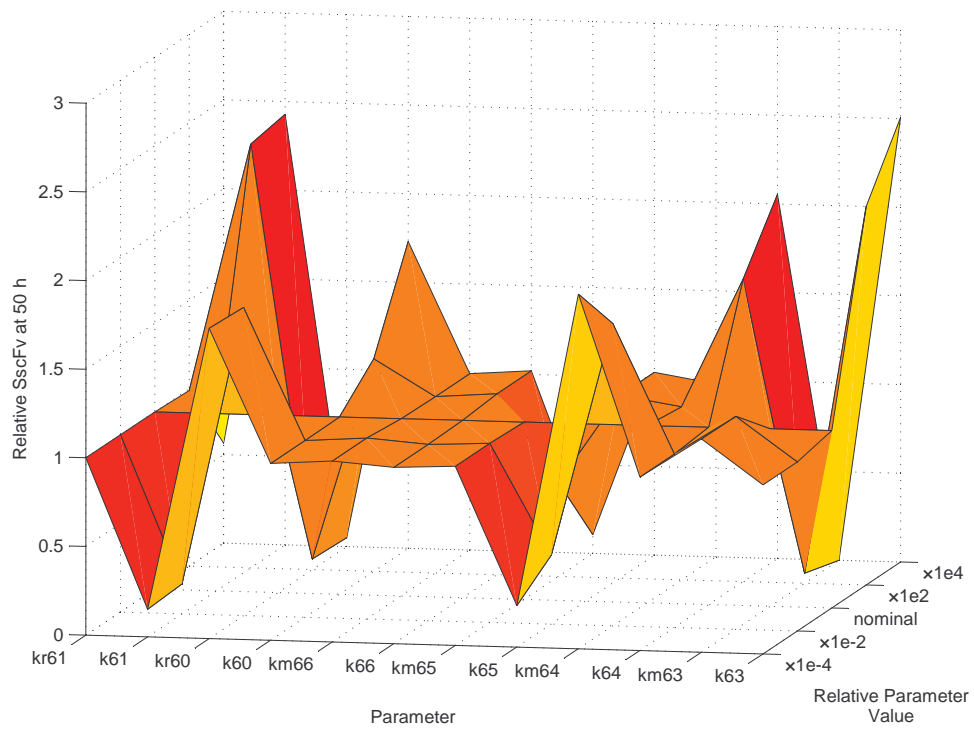


Figure 7:

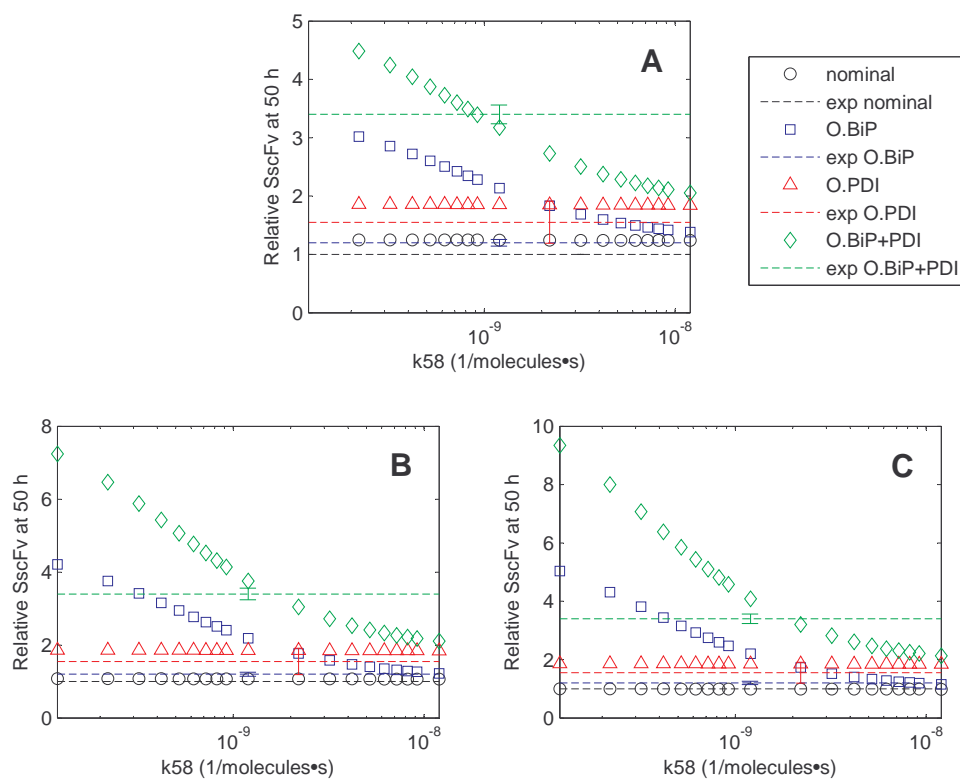


Figure 8:

Appendix

Parameter Derivations

- k_3/k_{63} , k_{m3}/k_{m63} , k_7/k_{64} , k_{m7}/k_{m64} , k_4/k_{65} , k_{m4}/k_{m65} , k_5/k_{66} , **and** k_{m5}/k_{m66} , **UscFv folding and misfolding rates.** For Fab antibody fragments, Mayer et al. (26) measured 2% nominal folding, 15% folding with BiP and ATP, 20% folding with PDI, and 40% folding with BiP, PDI, and ATP. These folding percentages were assumed to be loosely applicable to 4-4-20 scFv fragment folding, since Nieba et al. (50) has reported 2% nominal folding when the fragment is expressed in *Escherichia coli*. Freund et al. (51) measured a fast folding phase rate of $0.324 \frac{1}{\text{min}}$ and slow phase rate of $0.048 \frac{1}{\text{min}}$ for another scFv fragment. The overall folding rate

$$\left(\frac{1}{0.324 \frac{1}{\text{min}}} + \frac{1}{0.048 \frac{1}{\text{min}}} \right)^{-1} \frac{1 \text{ min}}{60 \text{ s}} = 7.0 \times 10^{-4} \frac{1}{\text{s}}$$

was assumed to be applicable to the 4-4-20 fragment, so this was the nominal and BiP-assisted folding rate (k_3/k_{63} and k_7/k_{64}) used in the mathematical models. The remaining folding rates could be derived from the collected information:

$$\frac{2\%}{98\%} = \frac{7.0 \times 10^{-4} \frac{1}{s}}{k_{m7}/k_{m64}, k_{m5}/k_{m66}} \Rightarrow k_{m7}/k_{m64}, k_{m4}/k_{m65}, k_{m5}/k_{m66} = 3.4 \times 10^{-2} \frac{1}{s} \quad (14)$$

$$\frac{15\%}{85\%} = \frac{7.0 \times 10^{-4} \frac{1}{s}}{k_{m3}/k_{m63}, k_{m4}/k_{m65}} \Rightarrow k_{m3}/k_{m63} = 3.9 \times 10^{-3} \frac{1}{s} \quad (15)$$

$$\frac{20\%}{80\%} = \frac{k_5/k_{66}}{3.4 \times 10^{-2} \frac{1}{s}} \Rightarrow k_5/k_{66} = 8.5 \times 10^{-3} \frac{1}{s} \quad (16)$$

$$\frac{50\%}{50\%} = \frac{k_4/k_{65}}{3.4 \times 10^{-2} \frac{1}{s}} \Rightarrow k_4/k_{65} = 3.4 \times 10^{-2} \frac{1}{s} \quad (17)$$

$$(18)$$

To accelerate folding dynamics, all of these rate constant values were multiplied by a factor of 10. Further, k_4/k_{65} was multiplied by another factor of 10 to emphasize the increase in folding rate caused by BiP *and* PDI binding.

- k_6/k_{60} , k_{r6}/k_{r60} , k_{69} , k_{r69} , k_2/k_{61} , k_{r2}/k_{r61} , k_{70} , k_{r70} , k_{76} , **and** k_{r76} , **BiP- and PDI-UscFv and general unfolded protein binding and dissociation rates.** k_6/k_{60} and k_{r6}/k_{r60} are taken directly from Robinson and Lauffenburger (65), with the original references provided in Table 2. Units conversion was implemented using $4.35 \times 10^{-15} \frac{L}{ER}$. BiP-general unfolded protein binding and release rates were taken directly from Hildebrandt et al. (64), which used an optimized value for binding, and the Robinson and Lauffenburger (65) value for release.

Darby and Creighton (47) measured a PDI binding rate of $600 \frac{1}{M \cdot s}$, which converts to $k_2/k_{61}, k_{70} = 2.3 \times 10^{-7} \frac{1}{molecules \cdot s}$. Primm and Gilbert (48) and Puig et al. (49) measured the dissociation constant

for various forms of PDI from various substrates to be about $1 \mu\text{M}$, which converts to 2.62×10^3 molecules. This value was used to calculate the dissociation rate: $k_{r2}/k_{r61}, k_{r70} = (2.62 \times 10^3 \text{ molecules})(2.3 \times 10^{-7} \frac{1}{\text{molecules}\cdot\text{s}}) = 6.0 \times 10^{-4} \frac{1}{\text{s}}$.

For PDI chaperone binding/dissociation, Gilbert (31) reviewed dissociation constants ranging from 50 to 1000 μM . The average of these values was used: 1.31×10^6 molecules, after units conversion. The chaperone binding rate was arbitrarily taken to be identical to the foldase binding rate ($k_{76} = 2.3 \times 10^{-7} \frac{1}{\text{molecules}\cdot\text{s}}$). The consequent chaperone release rate was then $3.2 \times 10^{-1} \frac{1}{\text{s}}$.

- **k_{55} , k_{56} , k_{58} , and k_{59} , scFv translation and transport rates.**

Ribbeck and Görlich (54), Siebrasse and Peters (55), and Smith et al. (56) place nuclear translocation at a rate of about $100 \frac{\text{MDa}}{\text{s}\cdot\text{NPC molecule}}$ in various vertebrates for various molecules. Ribbeck and Görlich (54) measured 2,800 NPC molecules in the nuclear envelope of HeLa cells. These values were combined to produce a general value for the nuclear translocation rate, $2.8 \times 10^5 \frac{\text{MDa}}{\text{s}}$, which was assumed to apply to *Saccharomyces cerevisiae*.

Calapez et al. (57), Lukacs et al. (58), Shav-Tal et al. (59), and Politz et al. (60) measured diffusion rates for a variety of species in the nucleus, including DNA, mRNA, and nascent ribosomes, to be on the order of $1 \frac{\mu\text{M}}{\text{s}}$. Given an estimated *Saccharomyces cerevisiae* nuclear volume of 1.74×10^{-15} L and an assumption of nuclear sphericity, the characteristic area ($\langle r^2 \rangle$) of the nucleus may be calculated:

$$\langle r^2 \rangle = \frac{3}{4\pi} 1.74 \times 10^{-15} \text{ L} \frac{10^{15} \mu\text{m}^3}{\text{L}}^{2/3} = 0.56 \mu\text{m}^2 \quad (19)$$

The resulting effective diffusion rate was then

$$1 \frac{\frac{\mu\text{M}}{\text{s}}}{0.56 \mu\text{m}^2} = 1.8 \frac{1}{\text{s}}. \quad (20)$$

Combining the diffusion rate with the nuclear translocation rate and the molecular weight of scFv mRNA (0.320024 MDa) gave an overall nuclear translocation rate of:

$$k_{55} = \left(\frac{1}{\frac{2.8 \times 10^5 \frac{\text{MDa}}{\text{s}}}{0.320024 \text{ MDa}}} + \frac{1}{1.8 \frac{1}{\text{s}}} \right)^{-1} = 1.8 \frac{1}{\text{s}}. \quad (21)$$

Although ribosome occupancy density does not necessarily scale linearly with mRNA length (62), this assumption was made for simplification purposes. Using extrapolation points from (62), ribosome occupancy density could be estimated from the 963 nt-long scFv fragment mRNA:

$$\frac{1.2 \frac{\text{ribosomes}}{100 \text{ nts}} - 0.14 \frac{\text{ribosomes}}{100 \text{ nts}}}{400 \text{ nts} - 3600 \text{ nts}} = \frac{1.2 \frac{\text{ribosomes}}{100 \text{ nts}} - X \frac{\text{ribosomes}}{100 \text{ nts}}}{400 \text{ nts} - 963 \text{ nts}} \Rightarrow X = 1.01 \frac{\text{ribosomes}}{100 \text{ nts}}. \quad (22)$$

From this density, it could be estimated that there is an average of 10

ribosomes on the scFv fragment mRNA. Freedman (61) estimated an overall translation rate of $2 \frac{\text{aa}}{\text{s}}$. The scFv fragment mRNA is 321 amino acids long, so the overall scFv translation rate is $k_{56} = 10 \text{ ribosomes} \times \frac{2 \frac{\text{aa}}{\text{s}}}{321 \text{ aa}} = 6.2 \times 10^{-2} \frac{1}{\text{s}}$.

Goder et al. (63) estimated SRP binding and trafficking to the translocon to take place at a rate of $3.4 \frac{1}{\text{s}}$. The parameter k_{58} also includes BiP binding at the translocon, which occurs at a rate of $k_6/k_{60} = 1.2 \times 10^{-8} \frac{1}{\text{molecules} \cdot \text{s}}$. Combining these two rates provides the overall rate constant:

$$k_{58} = \left(\frac{1}{\frac{1}{(3.4 \text{ s})(3.37 \times 10^5 \text{ BiP molecules})}} + \frac{1}{1.2 \times 10^{-8} \frac{1}{\text{molecules} \cdot \text{s}}} \right)^{-1} = 1.2 \times 10^{-8} \frac{1}{\text{molecules} \cdot \text{s}}. \quad (23)$$

The value in the table is optimized for desired secreted scFv dependencies on BiP and PDI levels, as discussed in the text.

Theoretical analyses by Elston (46) place translocation at a rate of about $100 \frac{\text{nm}}{\text{s}}$. The average length of an amino acid is 0.35 nm, and the scFv fragment protein length is 317 amino acids. Thus, k_{59} is $9.0 \times 10^{-1} \frac{1}{\text{s}}$.

- k_d/k_{3d} , **scFv mRNA degradation rate.** As an approximation for scFv mRNA degradation, Oliveira and McCarthy (52) gives half-lives for a variety of mRNA's ranging from 1.5 to 7.5 min. The average of 4.5 min gave a first-order rate constant of $\frac{\ln 2}{4.5 \text{ min}} \times \frac{1 \text{ min}}{60 \text{ s}} = 2.6 \times 10^{-3} \frac{1}{\text{s}}$,

which was used to for k_{3d} .

- k_{1b} , k_{1bit} , and k_{2b} , **developing models rates.** k_{1b} encompasses the processes involved with k_{55} , k_{56} , k_{58} , and k_{59} . k_{58} largely remained the rate-limiting step, so its derived value, $1.2 \times 10^{-8} \frac{1}{\text{molecules}\cdot\text{s}}$, was used in these models. k_{1bit} is the equivalent rate without BiP dependence, so this dependence may be removed by the multiplication by 3.37×10^5 BiP molecules. Thus, $k_{1bit} = 4.0 \times 10^{-3} \frac{1}{\text{s}}$. k_{2b} was taken to be k_5 / k_{66} , made PDI-dependent by dividing by 5.24×10^5 PDI molecules.

Model Equations

Model 1.

$$\frac{d[\text{UscFv}]}{dt} = k_{1b}[\text{scFv mRNA}][\text{BiP}] - k_{2b}[\text{UscFv}][\text{PDI}] \quad (24)$$

$$\frac{d[\text{SscFv}]}{dt} = k_{2b}[\text{UscFv}][\text{PDI}] \quad (25)$$

$$\frac{d[\text{SscFv}]_{SS}}{dt} = k_{1b}[\text{BiP}][\text{scFv mRNA}] \quad (26)$$

Model 2.

$$\frac{d[\text{UscFv}]}{dt} = k_{1b}[\text{scFv mRNA}][\text{BiP}] - k_{2b}[\text{UscFv}][\text{PDI}] - k_{m5}[\text{UscFv}] \quad (27)$$

$$\frac{d[\text{SscFv}]}{dt} = k_{2b}[\text{UscFv}][\text{PDI}] \quad (28)$$

$$\frac{d[\text{SscFv}]_{SS}}{dt} = \frac{k_{1b}[\text{BiP}][\text{scFv mRNA}][\text{PDI}]}{\frac{k_{m5}}{k_{2b}} + [\text{PDI}]} \quad (29)$$

Model 3.

$$\frac{d[\text{BiP} \cdot \text{UscFv}]}{dt} = k_1[\text{scFv mRNA}][\text{BiP}] + k_{r2}[\text{BiP} \cdot \text{PDI} \cdot \text{UscFv}] - k_2[\text{PDI}][\text{BiP} \cdot \text{UscFv}] - (k_3 + k_{m3})[\text{BiP} \cdot \text{UscFv}] \quad (30)$$

$$\frac{d[\text{BiP} \cdot \text{PDI} \cdot \text{UscFv}]}{dt} = k_2[\text{PDI}][\text{BiP} \cdot \text{UscFv}] - k_{r2}[\text{BiP} \cdot \text{PDI} \cdot \text{UscFv}] - (k_4 + k_{m4})[\text{BiPPDI} \cdot \text{UscFv}] \quad (31)$$

$$\frac{d[\text{BiP}]}{dt} = (k_3 + k_{m3})[\text{BiP} \cdot \text{UscFv}] + (k_4 + k_{m4})[\text{BiP} \cdot \text{PDI} \cdot \text{UscFv}] - k_1[\text{scFv mRNA}][\text{BiP}] \quad (32)$$

$$\frac{d[\text{PDI}]}{dt} = (k_4 + k_{m4})[\text{BiP} \cdot \text{PDI} \cdot \text{UscFv}] + k_{r2}[\text{BiP} \cdot \text{PDI} \cdot \text{UscFv}] - k_2[\text{PDI}][\text{BiP} \cdot \text{UscFv}] \quad (33)$$

$$\frac{d[\text{SscFv}]}{dt} = k_3[\text{BiP} \cdot \text{UscFv}] + k_4[\text{BiP} \cdot \text{PDI} \cdot \text{UscFv}] \quad (34)$$

$$\frac{d[\text{SscFv}]_{SS}}{dt} = \frac{k_1[\text{BiP}][\text{scFv mRNA}](k_3(k_{r2} + k_4 + k_{m4}) + k_2[\text{PDI}]k_4)}{(k_3 + k_{m3})(k_{r2} + k_4 + k_{m4}) + k_2[\text{PDI}](k_4 + k_{m4})} \quad (35)$$

Model 3*.

$$\frac{d[\text{Cyt. UscFv}]}{dt} = V_{\text{UscFv}} - k_d[\text{Cyt. UscFv}] - k_1[\text{Cyt. UscFv}][\text{BiP}] \quad (36)$$

$$\frac{d[\text{BiP} \cdot \text{UscFv}]}{dt} = k_1[\text{Cyt. UscFv}][\text{BiP}] + k_{r2}[\text{BiP} \cdot \text{PDI} \cdot \text{UscFv}] - k_2[\text{PDI}][\text{BiP} \cdot \text{UscFv}] - (k_3 + k_{m3})[\text{BiP} \cdot \text{UscFv}] \quad (37)$$

$$\frac{d[\text{BiP} \cdot \text{PDI} \cdot \text{UscFv}]}{dt} = k_2[\text{PDI}][\text{BiP} \cdot \text{UscFv}] - k_{r2}[\text{BiP} \cdot \text{PDI} \cdot \text{UscFv}] - (k_4 + k_{m4})[\text{BiP} \cdot \text{PDI} \cdot \text{UscFv}] \quad (38)$$

$$\frac{d[\text{BiP}]}{dt} = (k_3 + k_{m3})[\text{BiP} \cdot \text{UscFv}] + (k_4 + k_{m4})[\text{BiP} \cdot \text{PDI} \cdot \text{UscFv}] - k_1[\text{Cyt. UscFv}][\text{BiP}] \quad (39)$$

$$\frac{d[\text{PDI}]}{dt} = (k_4 + k_{m4})[\text{BiP} \cdot \text{PDI} \cdot \text{UscFv}] + k_{r2}[\text{BiP} \cdot \text{PDI} \cdot \text{UscFv}] - k_2[\text{PDI}][\text{BiP} \cdot \text{UscFv}] \quad (40)$$

$$\frac{d[\text{SscFv}]}{dt} = k_3[\text{BiP} \cdot \text{UscFv}] + k_4[\text{BiP} \cdot \text{PDI} \cdot \text{UscFv}] \quad (41)$$

$$\frac{d[\text{SscFv}]_{SS}}{dt} = \frac{V_{\text{UscFv}}k_1[\text{BiP}](k_3(k_{r2} + k_4 + k_{m4}) + k_2[\text{PDI}]k_4)}{(k_1[\text{BiP}] + k_d)((k_3 + k_{m3})(k_{r2} + k_4 + k_{m4}) + k_2[\text{PDI}](k_4 + k_{m4}))} \quad (42)$$

Model 4.

$$\frac{d[\text{UscFv}]}{dt} = k_{r6}[\text{BiP} \cdot \text{UscFv}] - k_6[\text{BiP}][\text{UscFv}] - (k_7 + k_{m7})[\text{UscFv}] \quad (43)$$

$$\begin{aligned} \frac{d[\text{BiP} \cdot \text{UscFv}]}{dt} = & k_1[\text{scFv mRNA}][\text{BiP}] + k_{r2}[\text{BiP} \cdot \text{PDI} \cdot \text{UscFv}] - k_2[\text{PDI}][\text{BiP} \cdot \text{UscFv}] \\ & + k_6[\text{BiP}][\text{UscFv}] - k_{r6}[\text{BiP} \cdot \text{UscFv}] - (k_3 + k_{m3})[\text{BiP} \cdot \text{UscFv}] \end{aligned} \quad (44)$$

$$\begin{aligned} \frac{d[\text{BiP} \cdot \text{PDI} \cdot \text{UscFv}]}{dt} = & k_2[\text{PDI}][\text{BiP} \cdot \text{UscFv}] - k_{r2}[\text{BiP} \cdot \text{PDI} \cdot \text{UscFv}] \\ & - (k_4 + k_{m4})[\text{BiP} \cdot \text{PDI} \cdot \text{UscFv}] \end{aligned} \quad (45)$$

$$\begin{aligned} \frac{d[\text{BiP}]}{dt} = & (k_3 + k_{m3})[\text{BiP} \cdot \text{UscFv}] + (k_4 + k_{m4})[\text{BiP} \cdot \text{PDI} \cdot \text{UscFv}] + k_{r6}[\text{BiP} \cdot \text{UscFv}] \\ & - k_6[\text{BiP}][\text{UscFv}] - k_1[\text{scFv mRNA}][\text{BiP}] \end{aligned} \quad (46)$$

$$\frac{d[\text{PDI}]}{dt} = (k_4 + k_{m4})[\text{BiP} \cdot \text{PDI} \cdot \text{UscFv}] + k_{r2}[\text{BiP} \cdot \text{PDI} \cdot \text{UscFv}] - k_2[\text{PDI}][\text{BiP} \cdot \text{UscFv}] \quad (47)$$

$$\frac{d[\text{SscFv}]}{dt} = k_7[\text{UscFv}] + k_3[\text{BiP} \cdot \text{UscFv}] + k_4[\text{BiP} \cdot \text{PDI} \cdot \text{UscFv}] \quad (48)$$

$$\frac{d[\text{SscFv}]_{SS}}{dt} = \frac{k_1[\text{BiP}][\text{scFv mRNA}] \quad k_3 + \frac{k_4 k_2 [\text{PDI}]}{k_{r2} + k_4 + k_{m4}} + \frac{k_7 k_{r6}}{k_6 [\text{BiP}] + k_7 + k_{m7}}}{k_{r6} \quad 1 - \frac{k_6 [\text{BiP}]}{k_6 [\text{BiP}] + k_7 + k_{m7}} \quad + k_2 [\text{PDI}] \quad 1 - \frac{k_{r2}}{k_{r2} + k_4 + k_{m4}} \quad + k_3 + k_{m3}} \quad (49)$$

Model 4*.

$$\frac{d[\text{Cyt. UscFv}]}{dt} = V_{UscFv} - k_d[\text{Cyt. UscFv}] - k_1[\text{Cyt. UscFv}][\text{BiP}] \quad (50)$$

$$\frac{d[\text{UscFv}]}{dt} = k_{r6}[\text{BiP} \cdot \text{UscFv}] - k_6[\text{BiP}][\text{UscFv}] - (k_7 + k_{m7})[\text{UscFv}] \quad (51)$$

$$\begin{aligned} \frac{d[\text{BiP} \cdot \text{UscFv}]}{dt} = & k_1[\text{Cyt. UscFv}][\text{BiP}] + k_{r2}[\text{BiP} \cdot \text{PDI} \cdot \text{UscFv}] - k_2[\text{PDI}][\text{BiP} \cdot \text{UscFv}] \\ & + k_6[\text{BiP}][\text{UscFv}] - k_{r6}[\text{BiP} \cdot \text{UscFv}] - (k_3 + k_{m3})[\text{BiP} \cdot \text{UscFv}] \quad (52) \end{aligned}$$

$$\begin{aligned} \frac{d[\text{BiP} \cdot \text{PDI} \cdot \text{UscFv}]}{dt} = & k_2[\text{PDI}][\text{BiP} \cdot \text{UscFv}] - k_{r2}[\text{BiP} \cdot \text{PDI} \cdot \text{UscFv}] \\ & - (k_4 + k_{m4})[\text{BiP} \cdot \text{PDI} \cdot \text{UscFv}] \quad (53) \end{aligned}$$

$$\begin{aligned} \frac{d[\text{BiP}]}{dt} = & (k_3 + k_{m3})[\text{BiP} \cdot \text{UscFv}] + (k_4 + k_{m4})[\text{BiP} \cdot \text{PDI} \cdot \text{UscFv}] + k_{r6}[\text{BiP} \cdot \text{UscFv}] \\ & - k_6[\text{BiP}][\text{UscFv}] - k_1[\text{Cyt. UscFv}][\text{BiP}] \quad (54) \end{aligned}$$

$$\frac{d[\text{PDI}]}{dt} = (k_4 + k_{m4})[\text{BiP} \cdot \text{PDI} \cdot \text{UscFv}] + k_{r2}[\text{BiP} \cdot \text{PDI} \cdot \text{UscFv}] - k_2[\text{PDI}][\text{BiP} \cdot \text{UscFv}] \quad (55)$$

$$\frac{d[\text{SscFv}]}{dt} = k_7[\text{UscFv}] + k_3[\text{BiP} \cdot \text{UscFv}] + k_4[\text{BiP} \cdot \text{PDI} \cdot \text{UscFv}] \quad (56)$$

$$\frac{d[\text{SscFv}]_{SS}}{dt} = \frac{V_{UscFv} k_1 [\text{BiP}] \quad k_3 + \frac{k_4 k_2 [\text{PDI}]}{k_{r2} + k_4 + k_{m4}} + \frac{k_7 k_{r6}}{k_6 [\text{BiP}] + k_7 + k_{m7}}}{(k_1 [\text{BiP}] + k_d) \quad k_{r6} \quad 1 - \frac{k_6 [\text{BiP}]}{k_6 [\text{BiP}] + k_7 + k_{m7}} + k_2 [\text{PDI}] \quad 1 - \frac{k_{r2}}{k_{r2} + k_4 + k_{m4}} + k_3 + k_{m3}} \quad (57)$$

Model 5.

$$\frac{d[\text{BiP} \cdot \text{UscFv}]}{dt} = k_1[\text{scFv mRNA}][\text{BiP}] + k_{r2}[\text{BiP} \cdot \text{PDI} \cdot \text{UscFv}] - k_2[\text{PDI}][\text{BiP} \cdot \text{UscFv}] - (k_3 + k_{m3})[\text{BiP} \cdot \text{UscFv}] \quad (58)$$

$$\frac{d[\text{PDI} \cdot \text{UscFv}]}{dt} = k_{r6}[\text{BiP} \cdot \text{PDI} \cdot \text{UscFv}] - k_6[\text{BiP}][\text{PDI} \cdot \text{UscFv}] - (k_5 + k_{m5})[\text{PDI} \cdot \text{UscFv}] \quad (59)$$

$$\begin{aligned} \frac{d[\text{BiP} \cdot \text{PDI} \cdot \text{UscFv}]}{dt} &= k_2[\text{PDI}][\text{BiP} \cdot \text{UscFv}] - k_{r2}[\text{BiP} \cdot \text{PDI} \cdot \text{UscFv}] \\ &+ k_6[\text{BiP}][\text{PDI} \cdot \text{UscFv}] - k_{r6}[\text{BiP} \cdot \text{PDI} \cdot \text{UscFv}] - (k_4 + k_{m4})[\text{BiP} \cdot \text{PDI} \cdot \text{UscFv}] \quad (60) \end{aligned}$$

$$\begin{aligned} \frac{d[\text{BiP}]}{dt} &= (k_3 + k_{m3})[\text{BiP} \cdot \text{UscFv}] + (k_4 + k_{m4})[\text{BiP} \cdot \text{PDI} \cdot \text{UscFv}] \\ &+ k_{r6}[\text{BiP} \cdot \text{PDI} \cdot \text{UscFv}] - k_6[\text{BiP}][\text{PDI} \cdot \text{UscFv}] - k_1[\text{scFv mRNA}][\text{BiP}] \quad (61) \end{aligned}$$

$$\begin{aligned} \frac{d[\text{PDI}]}{dt} &= (k_4 + k_{m4})[\text{BiP} \cdot \text{PDI} \cdot \text{UscFv}] + (k_5 + k_{m5})[\text{PDI} \cdot \text{UscFv}] \\ &+ k_{r2}[\text{BiP} \cdot \text{PDI} \cdot \text{UscFv}] - k_2[\text{PDI}][\text{BiP} \cdot \text{UscFv}] \quad (62) \end{aligned}$$

$$\frac{d[\text{SscFv}]}{dt} = k_3[\text{BiP} \cdot \text{UscFv}] + k_5[\text{PDI} \cdot \text{UscFv}] + k_4[\text{BiP} \cdot \text{PDI} \cdot \text{UscFv}] \quad (63)$$

$$\begin{aligned} \frac{d[\text{SscFv}]_{SS}}{dt} &= \frac{k_3 k_1 [\text{BiP}][\text{scFv mRNA}]}{k_2 [\text{PDI}] + k_3 + k_{m3}} + \frac{k_3 k_{r2}}{k_2 [\text{PDI}] + k_3 + k_{m3}} + k_4 + \frac{k_5 k_{r6}}{k_6 [\text{BiP}] + k_5 + k_{m5}} \cdot \\ &\left\{ \frac{k_1 [\text{BiP}][\text{scFv mRNA}] k_2 [\text{PDI}]}{(k_2 [\text{PDI}] + k_3 + k_{m3}) k_{r6} \left(1 - \frac{k_6 [\text{BiP}]}{k_6 [\text{BiP}] + k_5 + k_{m5}} \right) + k_{r2} \left(1 - \frac{k_2 [\text{PDI}]}{k_2 [\text{PDI}] + k_3 + k_{m3}} \right)} \right\} \quad (64) \end{aligned}$$

Model 5*.

$$\frac{d[\text{Cyt. UscFv}]}{dt} = V_{UscFv} - k_d[\text{Cyt. UscFv}] - k_1[\text{Cyt. UscFv}][\text{BiP}] \quad (65)$$

$$\begin{aligned} \frac{d[\text{BiP} \cdot \text{UscFv}]}{dt} = & k_1[\text{Cyt. UscFv}][\text{BiP}] + k_{r2}[\text{BiP} \cdot \text{PDI} \cdot \text{UscFv}] - k_2[\text{PDI}][\text{BiP} \cdot \text{UscFv}] \\ & - (k_3 + k_{m3})[\text{BiP} \cdot \text{UscFv}] \quad (66) \end{aligned}$$

$$\frac{d[\text{PDI} \cdot \text{UscFv}]}{dt} = k_{r6}[\text{BiP} \cdot \text{PDI} \cdot \text{UscFv}] - k_6[\text{BiP}][\text{PDI} \cdot \text{UscFv}] - (k_5 + k_{m5})[\text{PDI} \cdot \text{UscFv}] \quad (67)$$

$$\begin{aligned} \frac{d[\text{BiP} \cdot \text{PDI} \cdot \text{UscFv}]}{dt} = & k_2[\text{PDI}][\text{BiP} \cdot \text{UscFv}] - k_{r2}[\text{BiP} \cdot \text{PDI} \cdot \text{UscFv}] \\ & + k_6[\text{BiP}][\text{PDI} \cdot \text{UscFv}] - k_{r6}[\text{BiP} \cdot \text{PDI} \cdot \text{UscFv}] - (k_4 + k_{m4})[\text{BiP} \cdot \text{PDI} \cdot \text{UscFv}] \quad (68) \end{aligned}$$

$$\begin{aligned} \frac{d[\text{BiP}]}{dt} = & (k_3 + k_{m3})[\text{BiP} \cdot \text{UscFv}] + (k_4 + k_{m4})[\text{BiP} \cdot \text{PDI} \cdot \text{UscFv}] \\ & + k_{r6}[\text{BiP} \cdot \text{PDI} \cdot \text{UscFv}] - k_6[\text{BiP}][\text{PDI} \cdot \text{UscFv}] - k_1[\text{Cyt. UscFv}][\text{BiP}] \quad (69) \end{aligned}$$

$$\begin{aligned} \frac{d[\text{PDI}]}{dt} = & (k_4 + k_{m4})[\text{BiP} \cdot \text{PDI} \cdot \text{UscFv}] + (k_5 + k_{m5})[\text{PDI} \cdot \text{UscFv}] \\ & + k_{r2}[\text{BiP} \cdot \text{PDI} \cdot \text{UscFv}] - k_2[\text{PDI}][\text{BiP} \cdot \text{UscFv}] \quad (70) \end{aligned}$$

$$\frac{d[\text{SscFv}]}{dt} = k_3[\text{BiP} \cdot \text{UscFv}] + k_5[\text{PDI} \cdot \text{UscFv}] + k_4[\text{BiP} \cdot \text{PDI} \cdot \text{UscFv}] \quad (71)$$

$$\begin{aligned} \frac{d[\text{SscFv}]_{SS}}{dt} = & \frac{k_3 V_{UscFv} k_1 [\text{BiP}]}{(k_1 [\text{BiP}] + k_d) (k_2 [\text{PDI}] + k_3 + k_{m3})} + \frac{k_3 k_{r2}}{k_2 [\text{PDI}] + k_3 + k_{m3}} + k_4 + \frac{k_5 k_{r6}}{k_6 [\text{BiP}] + k_5 + k_{m5}} \cdot \\ & \left\{ \frac{V_{UscFv} k_1 [\text{BiP}] k_2 [\text{PDI}]}{(k_1 [\text{BiP}] + k_d) (k_2 [\text{PDI}] + k_3 + k_{m3})} \frac{1}{k_{r6}} - \frac{k_6 [\text{BiP}]}{k_6 [\text{BiP}] + k_5 + k_{m5}} + k_{r2} \frac{1}{k_2 [\text{PDI}] + k_3 + k_{m3}} \right\} \quad (72) \end{aligned}$$

Model 6.

$$\frac{d[\text{UscFv}]}{dt} = k_{r6}[\text{BiP} \cdot \text{UscFv}] - k_6[\text{BiP}][\text{UscFv}] - (k_7 + k_{m7})[\text{UscFv}] \quad (73)$$

$$\begin{aligned} \frac{d[\text{BiP} \cdot \text{UscFv}]}{dt} = & k_1[\text{scFv mRNA}][\text{BiP}] + k_{r2}[\text{BiP} \cdot \text{PDI} \cdot \text{UscFv}] - k_2[\text{PDI}][\text{BiP} \cdot \text{UscFv}] \\ & + k_6[\text{BiP}][\text{UscFv}] - k_{r6}[\text{BiP} \cdot \text{UscFv}] - (k_3 + k_{m3})[\text{BiP} \cdot \text{UscFv}] \end{aligned} \quad (74)$$

$$\frac{d[\text{PDI} \cdot \text{UscFv}]}{dt} = k_{r6}[\text{BiP} \cdot \text{PDI} \cdot \text{UscFv}] - k_6[\text{BiP}][\text{PDI} \cdot \text{UscFv}] - (k_5 + k_{m5})[\text{PDI} \cdot \text{UscFv}] \quad (75)$$

$$\begin{aligned} \frac{d[\text{BiP} \cdot \text{PDI} \cdot \text{UscFv}]}{dt} = & k_2[\text{PDI}][\text{BiP} \cdot \text{UscFv}] - k_{r2}[\text{BiP} \cdot \text{PDI} \cdot \text{UscFv}] + k_6[\text{BiP}][\text{PDI} \cdot \text{UscFv}] \\ & - k_{r6}[\text{BiP} \cdot \text{PDI} \cdot \text{UscFv}] - (k_4 + k_{m4})[\text{BiP} \cdot \text{PDI} \cdot \text{UscFv}] \end{aligned} \quad (76)$$

$$\begin{aligned} \frac{d[\text{BiP}]}{dt} = & (k_3 + k_{m3})[\text{BiP} \cdot \text{UscFv}] + (k_4 + k_{m4})[\text{BiP} \cdot \text{PDI} \cdot \text{UscFv}] \\ & + k_{r6}([\text{BiP} \cdot \text{UscFv}] + [\text{BiP} \cdot \text{PDI} \cdot \text{UscFv}]) - k_6[\text{BiP}]([\text{UscFv}] + [\text{PDI} \cdot \text{UscFv}]) - k_1[\text{scFv mRNA}][\text{BiP}] \end{aligned} \quad (77)$$

$$\begin{aligned} \frac{d[\text{PDI}]}{dt} = & (k_4 + k_{m4})[\text{BiP} \cdot \text{PDI} \cdot \text{UscFv}] + (k_5 + k_{m5})[\text{PDI} \cdot \text{UscFv}] \\ & + k_{r2}[\text{BiP} \cdot \text{PDI} \cdot \text{UscFv}] - k_2[\text{PDI}][\text{BiP} \cdot \text{UscFv}] \end{aligned} \quad (78)$$

$$\frac{d[\text{SscFv}]}{dt} = k_7[\text{UscFv}] + k_3[\text{BiP} \cdot \text{UscFv}] + k_5[\text{PDI} \cdot \text{UscFv}] + k_4[\text{BiP} \cdot \text{PDI} \cdot \text{UscFv}] \quad (79)$$

$$\frac{d[\text{SscFv}]_{SS}}{dt} = \left\{ k_3 + \frac{k_2[\text{PDI}]}{k_{r2} + k_{r6} \left(1 - \frac{k_6[\text{BiP}]}{k_6[\text{BiP}] + k_5 + k_{m5}} \right) + k_4 + k_{m4}} \right. \quad (80)$$

$$\left. k_4 + \frac{k_5 k_{r6}}{k_6[\text{BiP}] + k_5 + k_{m5}} + \frac{k_7 k_{r6}}{k_6[\text{BiP}] + k_7 + k_{m7}} \right\} \quad (81)$$

$$\left\{ \frac{k_1[\text{BiP}][\text{scFv mRNA}]}{k_{r6} \left(1 - \frac{k_6[\text{BiP}]}{k_6[\text{BiP}] + k_7 + k_{m7}} \right) + k_2[\text{PDI}] \left(1 - \frac{k_{r2}}{k_{r2} + k_{r6} \left(1 - \frac{k_6[\text{BiP}]}{k_6[\text{BiP}] + k_5 + k_{m5}} \right) + k_4 + k_{m4}} \right)} \right\} + k_3 + k_{m3} \quad (82)$$

Model 6*.

$$\frac{d[\text{Cyt. UscFv}]}{dt} = V_{UscFv} - k_d[\text{Cyt. UscFv}] - k_1[\text{Cyt. UscFv}][\text{BiP}] \quad (83)$$

$$\frac{d[\text{UscFv}]}{dt} = k_{r6}[\text{BiP} \cdot \text{UscFv}] - k_6[\text{BiP}][\text{UscFv}] - (k_7 + k_{m7})[\text{UscFv}] \quad (84)$$

$$\begin{aligned} \frac{d[\text{BiP} \cdot \text{UscFv}]}{dt} &= k_1[\text{Cyt. UscFv}][\text{BiP}] + k_{r2}[\text{BiP} \cdot \text{PDI} \cdot \text{UscFv}] - k_2[\text{PDI}][\text{BiP} \cdot \text{UscFv}] \\ &\quad + k_6[\text{BiP}][\text{UscFv}] - k_{r6}[\text{BiP} \cdot \text{UscFv}] - (k_3 + k_{m3})[\text{BiP} \cdot \text{UscFv}] \end{aligned} \quad (85)$$

$$\frac{d[\text{PDI} \cdot \text{UscFv}]}{dt} = k_{r6}[\text{BiP} \cdot \text{PDI} \cdot \text{UscFv}] - k_6[\text{BiP}][\text{PDI} \cdot \text{UscFv}] - (k_5 + k_{m5})[\text{PDI} \cdot \text{UscFv}] \quad (86)$$

$$\begin{aligned} \frac{d[\text{BiP} \cdot \text{PDI} \cdot \text{UscFv}]}{dt} &= k_2[\text{PDI}][\text{BiP} \cdot \text{UscFv}] - k_{r2}[\text{BiP} \cdot \text{PDI} \cdot \text{UscFv}] + k_6[\text{BiP}][\text{PDI} \cdot \text{UscFv}] \\ &\quad - k_{r6}[\text{BiP} \cdot \text{PDI} \cdot \text{UscFv}] - (k_4 + k_{m4})[\text{BiP} \cdot \text{PDI} \cdot \text{UscFv}] \end{aligned} \quad (87)$$

$$\begin{aligned} \frac{d[\text{BiP}]}{dt} &= (k_3 + k_{m3})[\text{BiP} \cdot \text{UscFv}] + (k_4 + k_{m4})[\text{BiP} \cdot \text{PDI} \cdot \text{UscFv}] \\ + k_{r6}([\text{BiP} \cdot \text{UscFv}] + [\text{BiP} \cdot \text{PDI} \cdot \text{UscFv}]) &- k_6[\text{BiP}]([\text{UscFv}] + [\text{PDI} \cdot \text{UscFv}]) - k_1[\text{Cyt. UscFv}][\text{BiP}] \end{aligned} \quad (88)$$

$$\begin{aligned} \frac{d[\text{PDI}]}{dt} &= (k_4 + k_{m4})[\text{BiP} \cdot \text{PDI} \cdot \text{UscFv}] + (k_5 + k_{m5})[\text{PDI} \cdot \text{UscFv}] \\ &\quad + k_{r2}[\text{BiP} \cdot \text{PDI} \cdot \text{UscFv}] - k_2[\text{PDI}][\text{BiP} \cdot \text{UscFv}] \end{aligned} \quad (89)$$

$$\frac{d[\text{SscFv}]}{dt} = k_7[\text{UscFv}] + k_3[\text{BiP} \cdot \text{UscFv}] + k_5[\text{PDI} \cdot \text{UscFv}] + k_4[\text{BiP} \cdot \text{PDI} \cdot \text{UscFv}] \quad (90)$$

$$\frac{d[\text{SscFv}]_{SS}}{dt} = \left\{ k_3 + \frac{k_2[\text{PDI}]}{k_{r2} + k_{r6} \left(1 - \frac{k_6[\text{BiP}]}{k_6[\text{BiP}] + k_5 + k_{m5}} \right) + k_4 + k_{m4}} \right\} \cdot \quad (91)$$

$$\left\{ k_4 + \frac{k_5 k_{r6}}{k_6[\text{BiP}] + k_5 + k_{m5}} + \frac{k_7 k_{r6}}{k_6[\text{BiP}] + k_7 + k_{m7}} \right\} \cdot \quad (92)$$

$$\left\{ \frac{V_{UscFv} k_1 [\text{BiP}] / (k_1 [\text{BiP}] + k_d)}{k_{r6} \left(1 - \frac{k_6[\text{BiP}]}{k_6[\text{BiP}] + k_7 + k_{m7}} \right) + k_2[\text{PDI}] \left(1 - \frac{k_{r2}}{k_{r2} + k_{r6} \left(1 - \frac{k_6[\text{BiP}]}{k_6[\text{BiP}] + k_5 + k_{m5}} \right) + k_4 + k_{m4}} \right)} \right\} + k_3 + k_{m3} \quad (93)$$

Model 7.

$$\frac{d[\text{UscFv}]}{dt} = k_{1bit}[\text{scFv mRNA}] + k_{r6}[\text{BiP} \cdot \text{UscFv}] - k_6[\text{BiP}][\text{UscFv}] - (k_7 + k_{m7})[\text{UscFv}] \quad (94)$$

$$\frac{d[\text{BiP} \cdot \text{UscFv}]}{dt} = k_{r2}[\text{BiP} \cdot \text{PDI} \cdot \text{UscFv}] - k_2[\text{PDI}][\text{BiP} \cdot \text{UscFv}] + k_6[\text{BiP}][\text{UscFv}] - k_{r6}[\text{BiP} \cdot \text{UscFv}] - (k_3 + k_{m3})[\text{BiP} \cdot \text{UscFv}] \quad (95)$$

$$\frac{d[\text{BiP} \cdot \text{PDI} \cdot \text{UscFv}]}{dt} = k_2[\text{PDI}][\text{BiP} \cdot \text{UscFv}] - k_{r2}[\text{BiP} \cdot \text{PDI} \cdot \text{UscFv}] - (k_4 + k_{m4})[\text{BiP} \cdot \text{PDI} \cdot \text{UscFv}] \quad (96)$$

$$\frac{d[\text{BiP}]}{dt} = (k_3 + k_{m3})[\text{BiP} \cdot \text{UscFv}] + (k_4 + k_{m4})[\text{BiP} \cdot \text{PDI} \cdot \text{UscFv}] + k_{r6}[\text{BiP} \cdot \text{UscFv}] - k_6[\text{BiP}][\text{UscFv}] \quad (97)$$

$$\frac{d[\text{PDI}]}{dt} = (k_4 + k_{m4})[\text{BiP} \cdot \text{PDI} \cdot \text{UscFv}] + k_{r2}[\text{BiP} \cdot \text{PDI} \cdot \text{UscFv}] - k_2[\text{PDI}][\text{BiP} \cdot \text{UscFv}] \quad (98)$$

$$\frac{d[\text{SscFv}]}{dt} = k_7[\text{UscFv}] + k_3[\text{BiP} \cdot \text{UscFv}] + k_4[\text{BiP} \cdot \text{PDI} \cdot \text{UscFv}] \quad (99)$$

$$\frac{d[\text{SscFv}]_{SS}}{dt} = \frac{k_7 k_{1bit}[\text{scFv mRNA}]}{k_6[\text{BiP}] + k_7 + k_{m7}} + \frac{k_7 k_{r6}}{k_6[\text{BiP}] + k_7 + k_{m7}} + k_3 + \frac{k_4 k_2[\text{PDI}]}{k_{r2} + k_4 + k_{m4}} \quad (100)$$

$$\left(\frac{k_6 k_{1bit}[\text{BiP}][\text{scFv mRNA}]}{(k_6[\text{BiP}] + k_7 + k_{m7}) \left(k_{r6} \left(1 - \frac{k_6[\text{BiP}]}{k_6[\text{BiP}] + k_7 + k_{m7}} \right) + k_2[\text{PDI}] \left(1 - \frac{k_{r2}}{k_{r2} + k_4 + k_{m4}} \right) + k_3 + k_{m3} \right)} \right) \quad (101)$$

Model 8.

$$\frac{d[\text{Cyt. UscFv}]}{dt} = V_{\text{UscFv}} - k_d[\text{Cyt. UscFv}] - k_1[\text{Cyt. UscFv}][\text{BiP}] \quad (102)$$

$$\frac{d[\text{UscFv}]}{dt} = k_{r2}[\text{PDI} \cdot \text{UscFv}] - k_2[\text{PDI}][\text{UscFv}] + k_{r6}[\text{BiP} \cdot \text{UscFv}] - k_6[\text{BiP}][\text{UscFv}] - (k_7 + k_{m7})[\text{UscFv}] \quad (103)$$

$$\begin{aligned} \frac{d[\text{BiP} \cdot \text{UscFv}]}{dt} &= k_1[\text{Cyt. UscFv}][\text{BiP}] + k_{r2}[\text{BiP} \cdot \text{PDI} \cdot \text{UscFv}] - k_2[\text{PDI}][\text{BiP} \cdot \text{UscFv}] \\ &\quad + k_6[\text{BiP}][\text{UscFv}] - k_{r6}[\text{BiP} \cdot \text{UscFv}] - (k_3 + k_{m3})[\text{BiP} \cdot \text{UscFv}] \end{aligned} \quad (104)$$

$$\begin{aligned} \frac{d[\text{PDI} \cdot \text{UscFv}]}{dt} &= k_2[\text{PDI}][\text{UscFv}] - k_{r2}[\text{PDI} \cdot \text{UscFv}] + k_{r6}[\text{BiP} \cdot \text{PDI} \cdot \text{UscFv}] \\ &\quad - k_6[\text{BiP}][\text{PDI} \cdot \text{UscFv}] - (k_5 + k_{m5})[\text{PDI} \cdot \text{UscFv}] \end{aligned} \quad (105)$$

$$\begin{aligned} \frac{d[\text{BiP} \cdot \text{PDI} \cdot \text{UscFv}]}{dt} &= k_2[\text{PDI}][\text{BiP} \cdot \text{UscFv}] - k_{r2}[\text{BiP} \cdot \text{PDI} \cdot \text{UscFv}] + k_6[\text{BiP}][\text{PDI} \cdot \text{UscFv}] \\ &\quad - k_{r6}[\text{BiP} \cdot \text{PDI} \cdot \text{UscFv}] - (k_4 + k_{m4})[\text{BiP} \cdot \text{PDI} \cdot \text{UscFv}] \end{aligned} \quad (106)$$

$$\frac{d[\text{BiP}]}{dt} = (k_3 + k_{m3})[\text{BiP} \cdot \text{UscFv}] + (k_4 + k_{m4})[\text{BiP} \cdot \text{PDI} \cdot \text{UscFv}]$$

$$+ k_{r6}([\text{BiP} \cdot \text{UscFv}] + [\text{BiP} \cdot \text{PDI} \cdot \text{UscFv}]) - k_6[\text{BiP}]([\text{UscFv}] + [\text{PDI} \cdot \text{UscFv}]) - k_1[\text{Cyt. UscFv}][\text{BiP}] \quad (107)$$

$$\frac{d[\text{PDI}]}{dt} = (k_4 + k_{m4})[\text{BiP} \cdot \text{PDI} \cdot \text{UscFv}] + (k_5 + k_{m5})[\text{PDI} \cdot \text{UscFv}]$$

$$+ k_{r2}([\text{PDI} \cdot \text{UscFv}] + [\text{BiP} \cdot \text{PDI} \cdot \text{UscFv}]) - k_2[\text{PDI}]([\text{UscFv}] + [\text{BiP} \cdot \text{UscFv}]) \quad (108)$$

$$\frac{d[\text{SscFv}]}{dt} = k_7[\text{UscFv}] + k_3[\text{BiP} \cdot \text{UscFv}] + k_5[\text{PDI} \cdot \text{UscFv}] + k_4[\text{BiP} \cdot \text{PDI} \cdot \text{UscFv}] \quad (109)$$

$$L = \frac{k_{r6}}{k_{r2} + k_6[\text{BiP}] + k_5 + k_{m5}} \quad (110)$$

$$M = \frac{k_6[\text{BiP}]}{k_6[\text{BiP}] - \frac{k_{r2}k_2[\text{PDI}]}{k_{r2} + k_6[\text{BiP}] + k_5 + k_{m5}} + k_2[\text{PDI}] + k_7 + k_{m7} (k_{r2} + k_6[\text{BiP}] + k_5 + k_{m5})} \quad (111)$$

$$D = k_{r2} - M k_{r2} k_2 [\text{PDI}] L - k_6 [\text{BiP}] L + k_{r6} + k_4 + k_{m4} \quad (112)$$

$$P = \frac{M (k_{r2} + k_6[\text{BiP}] + k_5 + k_{m5}) ((1 + M k_{r6}) k_{r2} k_2 [\text{PDI}] L) + k_{r2} k_2 [\text{PDI}] + M k_{r6} k_{r2} k_2 [\text{PDI}]}{D} \quad (113)$$

$$[\text{BiP} \cdot \text{UscFv}]_{SS} = \frac{k_1[\text{BiP}]V_{\text{UscFv}}}{(k_1[\text{BiP}] + k_d) (k_{r6} + k_2[\text{PDI}] + k_3 + k_{m3} - M k_{r6} (k_{r2} + k_6[\text{BiP}] + k_5 + k_{m5}) - P)} \quad (114)$$

$$[\text{UscFv}]_{SS} = k_{r6} + \frac{(1 + M k_{r6}) k_{r2} k_2 [\text{PDI}] L}{D} \frac{(M (k_{r2} + k_6[\text{BiP}] + k_5 + k_{m5})) [\text{BiP} \cdot \text{UscFv}]_{SS}}{k_6[\text{BiP}]} \quad (115)$$

$$[\text{BiP} \cdot \text{PDI} \cdot \text{UscFv}]_{SS} = \frac{(k_2[\text{PDI}] + M k_{r6} k_2 [\text{PDI}]) [\text{BiP} \cdot \text{UscFv}]_{SS}}{D} \quad (116)$$

$$[\text{PDI} \cdot \text{UscFv}]_{SS} = \frac{k_2[\text{PDI}][\text{UscFv}]_{SS} + k_{r6}[\text{BiP} \cdot \text{PDI} \cdot \text{UscFv}]_{SS}}{k_{r2} + k_6[\text{BiP}] + k_5 + k_{m5}} \quad (117)$$

$$\frac{d[\text{SscFv}]_{SS}}{dt} = k_7[\text{UscFv}]_{SS} + k_3[\text{BiP} \cdot \text{UscFv}]_{SS} + k_5[\text{PDI} \cdot \text{UscFv}]_{SS} + k_4[\text{BiP} \cdot \text{PDI} \cdot \text{UscFv}]_{SS} \quad (118)$$

Detailed Model

$$\frac{d[\text{BiP} \cdot \text{UP}]}{dt} = k_{69}[\text{BiP}][\text{UP}] - k_{r69}[\text{BiP} \cdot \text{UP}] + k_{r70}[\text{BiP} \cdot \text{PDI} \cdot \text{UP}] - k_{70}[\text{PDI}][\text{BiP} \cdot \text{UP}] \quad (119)$$

$$\begin{aligned} \frac{d[\text{BiP}]}{dt} = & k_{r60}([\text{BiP} \cdot \text{UscFv}] + [\text{BiP} \cdot \text{PDI} \cdot \text{UscFv}]) + k_{r69}([\text{BiP} \cdot \text{UP}] + [\text{BiP} \cdot \text{PDI} \cdot \text{UP}]) \\ & - (k_{58}[\text{cytoplasmic UscFv}] + k_{60}([\text{UscFv}] + [\text{PDI} \cdot \text{UscFv}]) + k_{69}([\text{UP}] + [\text{PDI} \cdot \text{UP}]))[\text{BiP}] \\ & + (k_{63} + k_{m63})[\text{BiP} \cdot \text{UscFv}] + (k_{65} + k_{m65})[\text{BiP} \cdot \text{PDI} \cdot \text{UscFv}] \quad (120) \end{aligned}$$

$$\frac{d[\text{UP}]}{dt} = k_{r69}[\text{BiP} \cdot \text{UP}] - k_{69}[\text{BiP}][\text{UP}] + k_{r76}[\text{PDI} \cdot \text{UP}] - k_{76}[\text{PDI}][\text{UP}] \quad (121)$$

$$\begin{aligned} \frac{d[\text{PDI}]}{dt} = & k_{r61}[\text{BiP} \cdot \text{PDI} \cdot \text{UscFv}] + k_{r70}[\text{BiP} \cdot \text{PDI} \cdot \text{UP}] + k_{r76}[\text{PDI} \cdot \text{UP}] \\ & - (k_{61}[\text{BiP} \cdot \text{UscFv}] + k_{70}[\text{BiP} \cdot \text{UP}] + k_{76}[\text{UP}])[\text{PDI}] \\ & + (k_{65} + k_{m65})[\text{BiP} \cdot \text{PDI} \cdot \text{UscFv}] + (k_{66} + k_{m66})[\text{PDI} \cdot \text{UscFv}] \quad (122) \end{aligned}$$

$$\frac{d[\text{nuclear scFv mRNA}]}{dt} = V_{scFv} - k_{55}[\text{nuclear scFv mRNA}] \quad (123)$$

$$\frac{d[\text{cytoplasmic scFv mRNA}]}{dt} = k_{55}[\text{nuclear scFv mRNA}] - k_{3d}[\text{cytoplasmic scFv mRNA}] \quad (124)$$

$$\begin{aligned} \frac{d[\text{cytoplasmic UscFv}]}{dt} = & k_{56}[\text{cytoplasmic scFv mRNA}] \\ & - k_{58}[\text{BiP}][\text{cytoplasmic UscFv}] - k_{57}[\text{cytoplasmic UscFv}] \quad (125) \end{aligned}$$

$$\frac{d[\text{ptt'ing UscFv}]}{dt} = k_{58}[\text{BiP}][\text{cytoplasmic UscFv}] - k_{59}[\text{ptt'ing UscFv}] \quad (126)$$

$$\begin{aligned} \frac{d[\text{BiP} \cdot \text{UscFv}]}{dt} = & k_{59}[\text{ptt'ing UscFv}] + k_{r61}[\text{BiP} \cdot \text{PDI} \cdot \text{UscFv}] - k_{61}[\text{PDI}][\text{BiP} \cdot \text{UscFv}] \\ & + k_{60}[\text{BiP}][\text{UscFv}] - k_{r60}[\text{BiP} \cdot \text{UscFv}] - (k_{63} + k_{m63})[\text{BiP} \cdot \text{UscFv}] \quad (127) \end{aligned}$$

$$\frac{d[\text{UscFv}]}{dt} = k_{r60}[\text{BiP} \cdot \text{UscFv}] - k_{60}[\text{BiP}][\text{UscFv}] - (k_{64} + k_{m64})[\text{UscFv}] \quad (128)$$

$$\frac{d[\text{MscFv}]}{dt} = k_{m64}[\text{UscFv}] + k_{m63}[\text{BiP} \cdot \text{UscFv}] + k_{m66}[\text{PDI} \cdot \text{UscFv}] + k_{m65}[\text{BiP} \cdot \text{PDI} \cdot \text{UscFv}] \quad (129)$$

$$\frac{d[\text{SscFv}]}{dt} = k_{64}[\text{UscFv}] + k_{63}[\text{BiP} \cdot \text{UscFv}] + k_{66}[\text{PDI} \cdot \text{UscFv}] + k_{65}[\text{BiP} \cdot \text{PDI} \cdot \text{UscFv}] \quad (130)$$

$$\begin{aligned} \frac{d[\text{BiP} \cdot \text{PDI} \cdot \text{UscFv}]}{dt} = & k_{61}[\text{PDI}][\text{BiP} \cdot \text{UscFv}] - k_{r61}[\text{BiP} \cdot \text{PDI} \cdot \text{UscFv}] + k_{60}[\text{BiP}][\text{PDI} \cdot \text{UscFv}] \\ & - k_{r60}[\text{BiP} \cdot \text{PDI} \cdot \text{UscFv}] - (k_{65} + k_{m65})[\text{BiP} \cdot \text{PDI} \cdot \text{UscFv}] \quad (131) \end{aligned}$$

$$\frac{d[\text{PDI} \cdot \text{UscFv}]}{dt} = k_{r60}[\text{BiP} \cdot \text{PDI} \cdot \text{UscFv}] - k_{60}[\text{BiP}][\text{PDI} \cdot \text{UscFv}] - (k_{66} + k_{m66})[\text{PDI} \cdot \text{UscFv}] \quad (132)$$

$$\frac{d[\text{BiP} \cdot \text{PDI} \cdot \text{UP}]}{dt} = k_{69}[\text{BiP}][\text{PDI} \cdot \text{UP}] - k_{r69}[\text{BiP} \cdot \text{PDI} \cdot \text{UP}] + k_{70}[\text{PDI}][\text{BiP} \cdot \text{UP}] - k_{r70}[\text{BiP} \cdot \text{PDI} \cdot \text{UP}] \quad (133)$$

$$\frac{d[\text{PDI} \cdot \text{UP}]}{dt} = k_{r69}[\text{BiP} \cdot \text{PDI} \cdot \text{UP}] - k_{69}[\text{BiP}][\text{PDI} \cdot \text{UP}] - k_{r76}[\text{PDI} \cdot \text{UP}] + k_{76}[\text{PDI}][\text{UP}] \quad (134)$$

References

1. Kitano, H., 2002. Systems Biology: A Brief Overview. *Science* 295:1662–1664.
2. Hasty, J., D. McMillen, F. Isaacs, and J. J. Collins, 2001. Computational Studies of Gene Regulatory Networks: In Numero Molecular Biology. *Nat Rev Genet* 2:268–279.
3. de Jong, H., 2002. Modeling and Simulation of Genetic Regulatory Systems: A Literature Review. *J Comput Biol* 9:67–103.
4. Smolen, P., D. A. Baxter, and J. H. Byrne, 2000. Mathematical Modeling of Gene Networks. *Neuron* 26:567–580.
5. Kholodenko, B. N., A. Kiyatkin, F. J. Bruggeman, E. Sontag, H. V. Westerhoff, and J. B. Hoek, 2002. Untangling the Wires: A Strategy to Trace Functional Interactions in Signaling and Gene Networks. *Proc Natl Acad Sci U S A* 99:12841–12846.
6. Forger, D. B., and C. S. Peskin, 2003. A Detailed Predictive Model of the Mammalian Circadian Clock. *Proc Natl Acad Sci U S A* 100:14806–14811.
7. Tyson, J. J., C. I. Hong, C. D. Thron, and B. Novak, 1999. A Simple Model of Circadian Rhythms Based on Dimerization and Proteolysis of PER and TIM. *Biophys J* 77:2411–2417.
8. Leloup, J.-C., and A. Goldbeter, 1998. A Model for Circadian Rhythms in *Drosophila* Incorporating the Formation of a Complex Between the PER and TIM Proteins. *J Biol Rhythms* 13:70–87.
9. Leloup, J.-C., and A. Goldbeter, 2003. Toward a Detailed Computational

- Model for the Mammalian Circadian Clock. *Proc Natl Acad Sci U S A* 100:7051–7056.
10. Aldridge, B. B., J. M. Burke, D. A. Lauffenburger, and P. K. Sorger, 2006. Physicochemical Modelling of Cell Signalling Pathways. *Nat Cell Biol* 8:1195–1203.
 11. Ideker, T., and D. Lauffenburger, 2003. Building with a Scaffold: Emerging Strategies for High- to Low-Level Cellular Modeling. *Trends Biotechnol* 21:255–262.
 12. Gardner, T. S., C. R. Cantor, and J. J. Collins, 2000. Construction of a Genetic Toggle Switch in *Escherichia coli*. *Nature* 403:339–403.
 13. Elowitz, M. B., and S. Leibler, 2000. A Synthetic Oscillatory Network of Transcriptional Regulators. *Nature* 403:335–338.
 14. Bornholdt, S., 2005. Systems Biology. Less is More in Modeling Large Genetic Networks. *Science* 310:449–451.
 15. III, C. A. L., J. T. Douglas, D. T. Curiel, and R. D. Alvarez, 2004. Single-Chain Antibodies: A Therapeutic Modality for Cancer Gene Therapy (Review). *Int J Oncol* 24:765–771.
 16. Mehren, M. V., and L. M. Weiner, 1996. Monoclonal Antibody-Based Therapy. *Curr Opin Oncol* 8:493–498.
 17. Shusta, E. V., R. T. Raines, A. Plückthun, and K. D. Wittrup, 1998. Increasing the Secretory Capacity of *Saccharomyces Cerevisiae* for Production of Single-Chain Antibody Fragments. *Nat Biotechnol* 16:773–777.
 18. Sudbery, P. E., 1996. The Expression of Recombinant Proteins in Yeasts. *Curr Opin Biotechnol* 7:517–524.

19. Verma, R., E. Boleti, and A. J. T. George, 1998. Antibody Engineering: Comparison of Bacterial, Yeast, Insect and Mammalian Expression Systems. *J Immunol Methods* 216:165–181.
20. Xu, P., D. Raden, F. J. D. III, and A. S. Robinson, 2005. Analysis of Unfolded Protein Response During Single-Chain Antibody Expression in *Saccharomyces cerevisiae* Reveals Different Roles for BiP and PDI in Folding. *Metab Eng* 7:269–279.
21. Guido, N. J., X. Wang, D. Adalsteinsson, D. McMillen, J. Hasty, C. R. Cantor, T. C. Elston, and J. J. Collins, 2006. A Bottom-Up Approach to Gene Regulation. *Nature* 439:856–860.
22. A.Hillson, D., N. Lambert, and R. B. Freedman, 1984. Formation and Isomerization of Disulfide Bonds in Proteins: Protein Disulfide-Isomerase. *Methods Enzymol* 107:281–294.
23. Ghaemmaghami, S., W. K. Huh, K. Bower, R. W. Howson, A. Belle, N. Dephoure, E. K. O’Shea, and J. S. Weissman, 2003. Global Analysis of Protein Expression in Yeast. *Nature* 425:737–741.
24. Lyles, M. M., and H. F. Gilbert, 1991. Catalysis of the Oxidative Folding of Ribonuclease A by Protein Disulfide Isomerase: Dependence of the Rate on the Composition of the Redox Buffer. *Biochemistry* 30:613–619.
25. Hampton, R. Y., 2002. ER-Associated Degradation in Protein Quality Control and Cellular Regulation. *Curr Opin Cell Biol* 14:476–482.
26. Mayer, M., U. Kies, R. Kammermeier, and J. Buchner, 2000. BiP and PDI Cooperate in the Oxidative Folding of Antibodies *in vitro*. *J. Biol. Chem.* 275:29421–29425.

27. Gething, M.-J., 1999. Role and Regulation of the ER Chaperone BiP. *Sem Cell Dev Biol* 10:465–472.
28. Puig, A., and H. F. Gilbert, 1994. Protein Disulfide Isomerase Exhibits Chaperone and Anti-Chaperone Activity in the Oxidative Refolding of Lysozyme. *J. Biol. Chem.* 269:7764–7771.
29. Song, J., and C. Wang, 1995. Chaperone-Like Activity of Protein Disulfide-Isomerase in the Refolding of Rhodanese. *Eur J Biochem* 231:312–316.
30. Yao, Y., Y. Zhou, and C. Wang, 1997. Both the Isomerase and Chaperone Activities of Protein Disulfide Isomerase are Required for the Reactivation of Reduced and Denatured Acidic Phospholipase A2. *EMBO J* 16:651–658.
31. Gilbert, H. F., 1997. Protein Disulfide Isomerase and Assisted Protein Folding. *J. Biol. Chem.* 272:29399–29402.
32. Xu, P., 2006. Sensing and Analyzing Unfolded Protein Response During Heterologous Protein Production. Ph.D. thesis, University of Delaware. Dissertation to the Faculty of the University of Delaware in partial fulfillment of the requirements for the degree of Doctor of Philosophy in Chemical Engineering.
33. Latterich, M., and R. Schekman, 1994. The Karyogamy Gene KAR2 and Novel Proteins Are Required for ER-Membrane Fusion. *Cell* 78:87–98.
34. Kitano, H., 2002. Computational Systems Biology. *Nature* 420:206–210.
35. Cary, M., G. Bader, and C. Sander, 2005. Pathway Information for Systems Biology. *FEBS Lett* 579:1815–1820.
36. HarshaRani, G., S. Vayttaden, and U. Bhalla, 2005. Electronic Data Sources for Kinetic Models of Cell Signaling. *J Biochem (Tokyo)* 137:653–657.

37. Hirschman, L., J. Park, J. Tsujii, L. Wong, and C. Wu, 2002. Accomplishments and Challenges in Literature Data Mining for Biology. *Bioinformatics* 18:1553–1561.
38. Hu, Z., M. Narayanaswamy, K. Ravikumar, K. Vijay-Shanker, and C. Wu, 2005. Literature Mining and Database Annotation of Protein Phosphorylation Using a Rule-Based System. *Bioinformatics* 21:2759–2765.
39. Sorokin, A., K. Paliy, A. Selkov, O. V. Demin, S. Dronov, P. Ghazal, and I. Goryanin, 2006. The Pathway Editor: A Tool for Managing Complex Biological Networks. *IBM J Res & Dev* 50:561–573.
40. Conzelmann, H., J. Saez-Rodriguez, T. Sauter, E. Bullinger, F. Allgöwer, and E. Gilles, 2004. Reduction of Mathematical Models of Signal Transduction Networks: Simulation-Based Approach Applied to EGF Receptor Signalling. *Syst Biol (Stevenage)* 1:159–169.
41. Androulakis, I., 2000. Kinetic Mechanism Reduction Based on an Integer Programming Approach. *AIChE Journal* 46:361–371.
42. Maurya, M., V. V. S.J. Bornheimer, and S. Subramaniam, 2005. Reduced-Order Modelling of Biochemical Networks: Application to the GTPase-Cycle Signalling Module. *IEE Proc-Syst Biol* 152:229–242.
43. Okino, M., and M. Mavrovouniotis, 1998. Simplification of Mathematical Models of Chemical Reaction Systems. *Chem Rev* 98:391–408.
44. Taylor, S., F. D. III, and L. Petzold. Model Reduction Preserving the Phase Reponse Behavior of A Circadian Clock In preparation.
45. Flynn, G. C., T. G. Chappell, and J. E. Rothman, 1989. Peptide Binding and Release by Proteins Implicated as Catalysts of Protein Assembly. *Science* 245:385–390.

46. Elston, T. C., 2002. The Brownian Ratchet and Power Stroke Models for Post-translational Protein Translocation Into the Endoplasmic Reticulum. *Biophys. J.* 82:1239 – 1253.
47. Darby, N. J., and T. E. Creighton, 1995. Characterization of the Active Site Cysteine Residues of the Thioredoxin-Like Domains of Protein Disulfide Isomerase. *Biochemistry* 34:16770–16780.
48. Primm, T. P., and H. F. Gilbert, 2001. Hormone Binding by Protein Disulfide Isomerase, a High Capacity Hormone Reservoir of the Endoplasmic Reticulum. *J. Biol. Chem.* 276:281–286.
49. Puig, A., T. P. Primm, R. Surendran, J. C. Lee, K. D. Ballard, R. S. Orkiszewski, V. Makarov, and H. F. Gilbert, 1997. A 21-kDa C-Terminal Fragment of Protein-Disulfide Isomerase Has Isomerase, Chaperone, and Anti-Chaperone Activities. *J. Biol. Chem.* 272:32988–32994.
50. Nieba, L., A. Honegger, C. Krebber, and A. Plückthun, 1997. Disrupting the Hydrophobic Patches at the Antibody Variable/Constant Domain Interface: Improved *in vivo* Folding and Physical Characterization of an Engineered scFv Fragment. *Protein Engng.* 10:435–444.
51. Freund, C., A. Honegger, P. Hunziker, T. A. Holak, and A. Plückthun, 1996. Folding Nuclei of the scFv Fragment of an Antibody. *Biochemistry* 35:8457–8464.
52. Oliveira, C. C., and J. E. G. McCarthy, 1995. The Relationship Between Eukaryotic Translation and mRNA Stability. *J. Biol. Chem.* 270:8936–8943.
53. Liberek, K., J. Marszalek, D. Ang, C. Georgopoulos, and M. Zylicz, 1991. Escherichia Coli DnaJ and GrpE Heat Shock Proteins Jointly Stimulate ATPase Activity of DnaK. *Proc. Natl. Acad. Sci. U.S.A.* 88:2874–2878.

54. Ribbeck, K., and D. Görlich, 2001. Kinetic Analysis of Translocation Through Nuclear Pore Complexes. *EMBO J.* 20:1320–1330.
55. Siebrasse, J. P., and R. Peters, 2002. Rapid Translocation of NTF2 Through the Nuclear Pore of Isolated Nuclei and Nuclear Envelopes. *EMBO Reports* 3:887–892.
56. Smith, A. E., B. M. Slepchenko, J. C. Schaff, L. M. Loew, and I. G. Macara, 2002. Systems Analysis of Ran Transport. *Science* 295:488–491.
57. Calapez, A., H. M. Pereira, A. Calado, J. Braga, J. Rino, C. Carvalho, J. P. Tavanez, E. Wahle, A. C. Rosa, and M. Carmo-Fonseca, 2002. The Intranuclear Mobility of Messenger RNA Binding Proteins is ATP Dependent and Temperature Sensitive. *J. Cell. Biol.* 159:795–805.
58. Lukacs, G. L., P. Haggie, O. Seksek, D. Lechardeur, N. Freedman, and A. S. Verkman, 2000. Size-Dependent DNA Mobility in Cytoplasm and Nucleus. *J. Biol. Chem.* 275:1625–1629.
59. Shav-Tal, Y., X. Darzacq, S. M. Shenoy, D. Fusco, S. M. Janicki, D. L. Spector, and R. H. Singer, 2004. Dynamics of Single mRNPs in Nuclei of Living Cells. *Science* 304:1797–1800.
60. Politz, J. C. R., R. A. Tuft, and T. Pederson, 2003. Diffusion-Based Transport of Nascent Ribosomes in the Nucleus. *Mol. Biol. Cell* 14:4805–4812.
61. Freedman, R. B., 1992. Protein Folding in the Cell. W. H. Freeman and Co., New York.
62. Arava, Y., Y. Wang, J. D. Storey, C. L. Liu, P. O. Brown, and D. Herschlag, 2003. Genome-Wide Analysis of mRNA Translation Profiles in *Saccharomyces cerevisiae*. *Proc. Natl. Acad. Sci. USA* 100:3889–3894.

63. Goder, V., P. Crottet, and M. Spiess, 2000. In Vivo Kinetics of Protein Targeting to the Endoplasmic Reticulum Determined by Site-Specific Phosphorylation. *EMBO J.* 19:6704–6712.
64. Hildebrandt, S., D. Raden, A. S. Robinson, and F. J. D. 3rd. Sensitivity Analysis Discriminates Between Ire1p Activation Regulation Models in *S. cerevisiae*. *Submitted* .
65. Robinson, A., and D. Lauffenburger, 1996. Model for ER Chaperone Dynamics and Secretory Protein Interactions. *AIChE Journal* 42:1443–1453.